https://doi.org/10.5194/egusphere-2026-2493
Preprint. Discussion started: 1 June 2026

Modeling seismic site response to improve lacustrine paleoseismic records

Huitong Yang[1], Katleen Wils[1], Ariana Molenaar[2], Jasper Moernaut[2], Lei Wu[3], Roberto Urrutia[4], Mario Pino[5], Maarten Van Daele[1]

[1]Renard Centre of Marine Geology, Department of Geology, Ghent University, Ghent, Belgium.
[2]Institute of Geology, University of Innsbruck, Innsbruck, Austria.
[3]School of Earth Sciences, Zhejiang University, Hangzhou, China.
[4]Faculty of Environmental Sciences, University of Concepción, Concepción, Chile.
[5]Fundación para los Estudios Patrimoniales Pleistocenos de Osorno, Osorno, Chile.

Corresponding author: Huitong Yang (Huitong.Yang@UGent.be)

Abstract. Linking earthquake-triggered sedimentary imprints in lakes to ground motion parameters is essential for quantitative paleoseismology. However, current approaches rely on empirical ground motion prediction equations (GMPEs) and use a single time-averaged shear-wave velocity (V_{s30}) as a simplified site response proxy for a whole lake. We established a 3D shear velocity model to compute site-specific GMPE predictions and applied 2D numerical site response simulations for Lake Riñihue, Chile, to evaluate local ground motions for the 1960 M_w 9.5 Valdivia and 2010 M_w 8.8 Maule earthquakes. Even with site-specific V_{s30} inputs, 2D simulations predict peak ground accelerations (PGA) and peak ground velocities (PGV) that exceed GMPE estimates by more than a factor of two. By stepwise modification of model properties and testing additional flat-layered reference models, we demonstrate that impedance contrasts between stratigraphic units influence overall ground motion amplification, whereas multi-scale basin geometry controls its spatial distribution, generating localized ground motion spikes. Earthquake shaking in lakes can produce surficial sediment remobilization (SSR) and soft-sediment deformation structures (SSDS) in-situ. Comparison of site-specific ground motions with sedimentary records from lake cores shows that SSR and SSDS are independent processes controlled by different ground motion components. SSR depth is primarily controlled by slope angle and PGV, with its patchy spatial occurrence reflecting frequency-dependent site response, whereas SSDS is controlled by PGA, with different thresholds for progressively increasing deformation types, while also predicts deformation thickness. Our findings highlight that site-specific ground motion reconstruction is essential to accurately link ground motion parameters to lacustrine sedimentary imprints.

1 Introduction

Lake sediments can preserve continuous records of past earthquakes through mass-transport deposits (MTDs) (e.g., Kremer et al., 2017; Strasser et al., 2006; Moernaut et al., 2009; Praet et al., 2017), turbidites (e.g., Monecke et al., 2004; Moernaut et al., 2014; Howarth et al., 2014; Gastineau et al., 2024; Vandekerkhove et al., 2020), and soft-sediment deformation structures (SSDS) (e.g., Molenaar et al., 2022; Molenaar et al., 2024; Monecke et al., 2004; Avşar et al., 2016; Lu et al., 2020; RodríGuez-Pascua et al., 2000). While these archives have been used to extend earthquake chronologies beyond instrumental and historical records, linking sedimentary imprints to quantitative ground-motion parameters remains a

https://doi.org/10.5194/egusphere-2026-2493
Preprint. Discussion started: 1 June 2026

challenge, even though these relationships are crucial if we want to eventually use these sedimentary imprints to reconstruct earthquake source parameters and consider them for seismic hazard models (e.g., Vanneste et al., 2018; Lemot et al., 2024; Niederstätter et al., 2025; Howarth et al., 2021; Moernaut et al., 2025; Daxer et al., 2022). Previous studies have related different lacustrine earthquake deposits to ground motion parameters including peak ground acceleration (PGA) (e.g., Strasser et al., 2007; Meunier et al., 2007; Avşar et al., 2016), peak ground velocity (PGV) and shaking duration (e.g., Molenaar et al., 2021; Wils et al., 2026; Molenaar et al., 2024). For example, surficial sediment remobilization appear to be controlled predominantly by PGV and duration (Wils et al., 2026), whereas SSDS deformation degree increases with PGA and high-frequency shaking content (Molenaar et al., 2021; Wetzler et al., 2010; Lu et al., 2020; Molenaar et al., 2024). These empirical relationships are an important step towards quantitative paleoseismology, yet they are limited by how accurate local ground motions can currently be determined. In addition to the field-based studies, few studies have explored local lacustrine earthquake responses using numerical simulations or analogue models.

Most previous studies attempting at calibrating the lacustrine paleoseismograph rely on empirical ground motion prediction equations (GMPEs) or intensity prediction equations (IPEs) to calculate local shaking strength at a lake, assigning a single value to the entire lake (e.g., Wils et al., 2026; Molenaar et al., 2021; Kremer et al., 2017; Avşar et al., 2016; Howarth et al., 2014). While such approach provides a reasonable first approximation, it assumes spatially uniform shaking and does not reflect potential variability within a basin as a result of site effects that may influence the sedimentary record. Typically these GMPEs calculate shaking intensity as a function of earthquake magnitude, source-to-site distance, and a site term presented by the shear-wave velocity in the upper 30 m (V_{s30}) (Borcherdt, 1994; Montalva et al., 2017; Montalva et al., 2022). However, by applying a single V_{s30} value (and with a single fundamental frequency (f_0)) to an entire lake basin, spatial variations in ground motion caused by basin amplification effects, topography or lateral changes in subsurface structure are neglected. Thus the realistic spatial variations in ground motion remain poorly constrained and make it difficult to translate sedimentary earthquake imprints into robust ground motions. Even when considering spatially variable site conditions using different V_{s30} values, this still simplifies subsurface structure (Castellaro et al., 2008; Pitilakis et al., 2013). In particular, V_{s30} does not account for the full vertical velocity profile, impedance contrasts between individual layers, or basin geometry – even though these factors are known to control seismic wave amplification or attenuation in sediment-filled basins (Bard and Bouchon, 1985; Semblat et al., 2005). The use of GMPEs could thus lead to biased ground motion estimates, especially in settings with strong lateral variability in stratigraphy and topography such as in lake slopes and basins. To better estimate site-specific ground motions, physics-based numerical simulations offer a useful complement to GMPE-based estimates. Two-dimensional numerical models incorporate the stratigraphic parameters and basin structure influencing seismic amplification (Semblat et al., 2002; Taborda and Roten, 2015), yet they have so far not been applied in lacustrine settings.

Establishing quantitative correlations between ground motions and sedimentary imprints is further complicated by variability in geotechnical properties of lake sediments (e.g., consolidation, density, cohesion, and shear strength) and slope

https://doi.org/10.5194/egusphere-2026-2493
Preprint. Discussion started: 1 June 2026

morphology between different lakes. Previous multi-lake studies show that these factors influence the sensitivity to both SSDS formation and surficial sediment remobilization (e.g., Niederstätter et al (in review); Molenaar et al., 2021; Molenaar et al., 2022; Molenaar et al., 2024; Wils et al., 2026), making it difficult to isolate the effect of ground motions alone. Even within individual lakes, sediment characteristics may vary over time. As a result, sedimentary responses to different paleoseismic events not only reflect differences in ground motion, but also time-dependent variations in lithology, complicating direct comparisons between events.

Lake Riñihue in south-central Chile offers an ideal setting to test the influence of lake basin morphology on local ground motions. The lake experienced two well-documented megathrust earthquakes: the 1960 M_w 9.5 Valdivia and 2010 M_w 8.8 Maule events, for both of which the source parameters are well constrained (Moreno et al., 2009; Campos, 1984; Moernaut et al., 2014). Previous studies have documented the spatial distribution of different types of sedimentary imprints from both earthquakes across the basin (e.g., Molenaar et al., 2021; Molenaar et al., 2022; Van Daele et al., 2015; Moernaut et al., 2019), providing detailed observations that allow for comparisons between (the absence of) earthquake imprints and ground-motion patterns. Additionally, high resolution seismic reflection profiles collected in previous studies (Moernaut and De Batist, 2011; Moernaut et al., 2017) reveal the detailed subsurface stratigraphy and lithological variations within the lake basin. These seismic interpretations enable the construction of a shear-wave velocity model, and thus high-resolution V_{s30} maps, as well as physics-based ground motion simulations, rather than relying solely on GMPEs for ground motion estimations.

In this study, we develop a 3D stratigraphic and shear-wave velocity model for Lake Riñihue that enables us to compute site-specific ground motions using empirical GMPEs while considering spatially variable V_{s30} (and f_0) values, as well as develop two-dimensional site response simulations that additionally capture basin geometry and impedance contrasts to further refine local ground motion results. Our study is the first to compare empirical GMPEs with physics-based numerical simulations, showing that GMPEs using V_{s30} typically underestimate local ground motions in lacustrine basins. We further evaluate how the local ground motions relate to surficial remobilization and SSDS characteristics, allowing us to disentangle the primary controls on each process and derive quantitative constraints on earthquake imprints recorded in lake sediments.

2 Setting

Lake Riñihue is located along the Valdivia Segment of the Chilean subduction zone (Figure 1a), where the Nazca Plate subducts beneath the South American Plate at ~7.4 cm yr^{-1} (Demets et al., 2010). The M_w 9.5 1960 Valdivia earthquake fully ruptured this 1000 km long megathrust segment with a maximum coseismic slip of about 40 m (Moreno et al., 2009; Cifuentes, 1989; Campos, 1984), producing seismic intensities of VII–VIII around the lake (Astroza and Lazo, 2008). The more recent M_w 8.8 2010 Maule earthquake ruptured the adjacent tectonic segment to the north, with its southern tip

https://doi.org/10.5194/egusphere-2026-2493
Preprint. Discussion started: 1 June 2026

extending to ~100 km distance from the lake. The Valdivia Segment, or at least part of it, has also ruptured in 1575, 1737, and 1837 CE (Lomnitz, 2004).

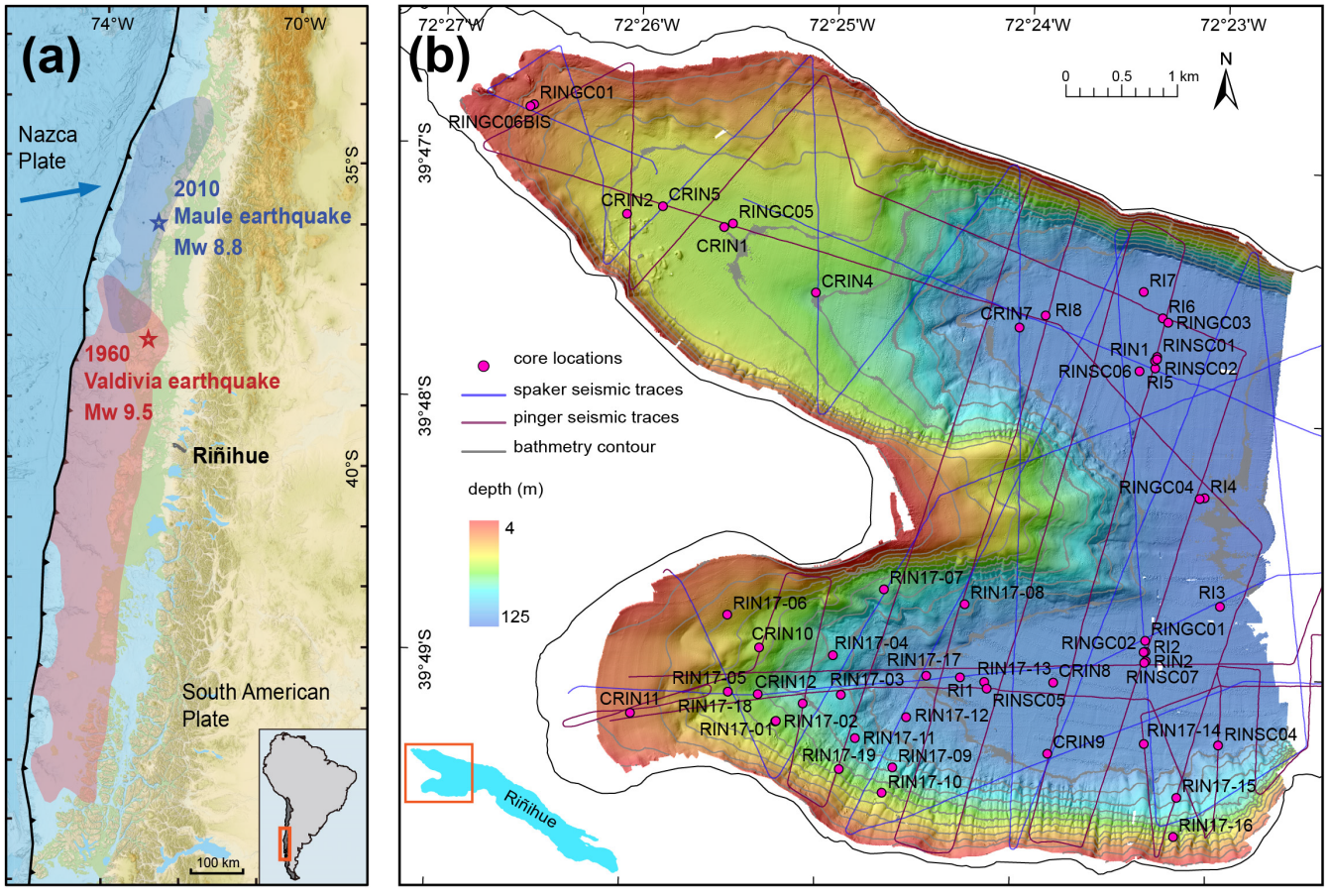

Figure 1. Geological settings. (a) A simplified map of the South Central Chilean subduction zone where the Nazca Plate subducts beneath the South American Plate (see inset for location). Colored zones indicate the rupture areas of the 2010 Mw 8.8 Maule earthquake and the 1960 Mw 9.5 Valdivia earthquake. The black solid line with small triangles is the subduction zone. (b) Bathymetric map of the western basin of Lake Riñihue with 20 m contour intervals. The red line marks the location of the seismic profile shown in Figure 2.

Lake Riñihue is a glacigenic piedmont lake located at the foot of the Andes (Figure 1b). It is approximately 28 km long and 2–5 km wide, with a maximum water depth of 323 m. Its sedimentary infill consists of three seismic-stratigraphic units, from top to bottom: Holocene lacustrine sediments, glaciolacustrine deposits and glacial till (Moernaut et al., 2017; Heirman, 2011). The Holocene background sedimentation in Lake Riñihue is characterized by biogenic varves with mean accumulation rates of ~1 mm yr^{-1} with Holcene sediment up to ~40 m and a total sediment thickness up to ~100 m in the central basin, intercalated with volcanic deposits from the nearby active volcanoes. The studied subbasin has no direct river inflows, and therefore sedimentary event deposits can be attributed to seismic triggering. Three types of earthquake-related

https://doi.org/10.5194/egusphere-2026-2493
Preprint. Discussion started: 1 June 2026

imprints have been identified: turbidites in basin sequences, centimeter-scale stratigraphic gaps from surficial sediment remobilization on slopes, and soft-sediment deformation structures (e.g., Moernaut et al., 2017; Molenaar et al., 2021; Molenaar et al., 2022).

3 Methods

3.1 Lake Basin Geological Model

3.1.1 Seismic Reflection Profiles

High-resolution reflection-seismic data were acquired in Lake Riñihue in 2007 by the Renard Centre of Marine Geology (RCMG; Ghent University), using two seismic systems: a CENTIPEDE sparker (0.4–1.5 kHz) with a single-channel streamer and a GEOPULSE pinger (~3.5 kHz) (Figure 1b). The sparker data allowed imaging of the entire sedimentary infill with a vertical resolution of about 37–75 cm, while the pinger system provided higher resolution of about 10–20 cm of the upper 15-20 m. These seismic data were imported into S&P Global Kingdom Suite software for detailed visualization and stratigraphic interpretation. Previous interpretations of these seismic data by Moernaut et al. (2017) and Heirman (2011) provide the foundation for our analysis. As such, four major seismic-stratigraphic units were identified and traced across all seismic profiles (Figure 2): From top to bottom, (1) Holocene lacustrine sediments with thickness ranging from 0 to 40 m (laminated silts and diatom-rich sediments), (2) glaciolacustrine deposits, (3) glacial till, and (4) the lowermost bedrock basement. We revisited these datasets with a focus on developing a seismic-stratigraphic framework that distinguishes units based on lithological variations, thus corresponding to different shear-wave velocities within the lake basin. The stratigraphic interfaces between these four major units as well as the lake floor and three internal unit boundaries were digitized at 5 m intervals along each profile.

https://doi.org/10.5194/egusphere-2026-2493
Preprint. Discussion started: 1 June 2026

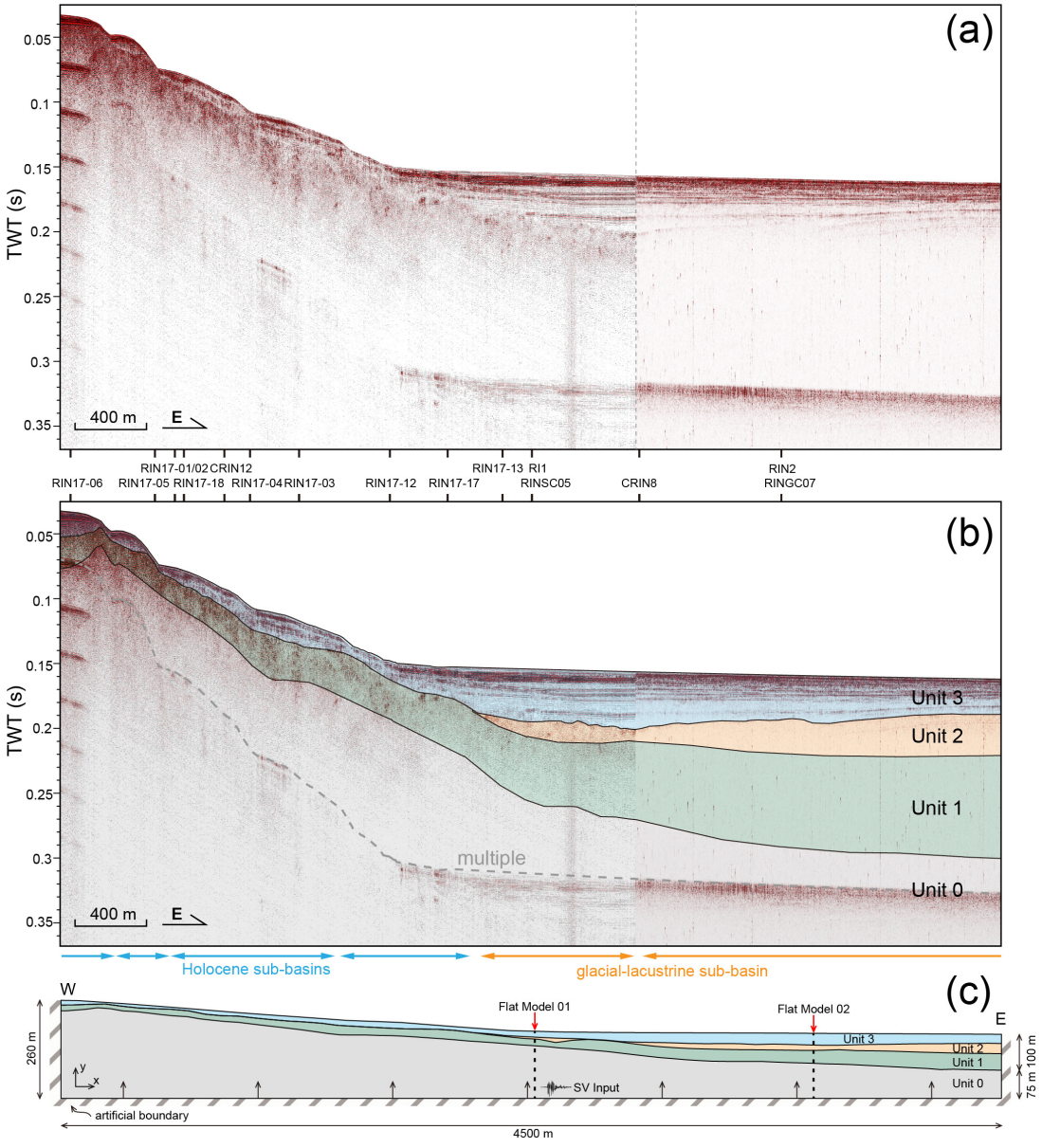

Figure 2. West-east seismic reflection profile across the western basin of Lake Riñihue, combining sparker (left) and pinger (right) data (location shown in Figure 1b). (a) Uninterpreted seismic profile. The dashed gray line marks a spliced section where two seismic lines were joined. (b) Interpreted seismic stratigraphy showing four seismic-stratigraphic units: Unit 3 (Holocene sediments), Unit 2 (glaciolacustrine deposits), Unit 1 (glacial till), and Unit 0 (bedrock basement). The dashed gray line indicates seismic multiple. Blue and orange arrows delineate Holocene sub-basins on the slopes and glaciolacustrine sub-basins range, respectively. (c) Sketch map of the 2D numerical model for site response simulations. The model is 4500 m wide and 260 m deep, with basin geometry from the seismic stratigraphy. Four units properties are listed in Table 1. Vertically incident SV-waves are applied at the base (upward arrows), with viscous dashpot absorbing boundaries at the base and lateral edges. Red arrows show the locations of flat-layered reference models FM01 and FM02.

https://doi.org/10.5194/egusphere-2026-2493
Preprint. Discussion started: 1 June 2026

3.1.2 Shear-wave Velocity Model

Based on the seismic-stratigraphic interpretation, we developed a 3D shear-wave velocity model for Lake Riñihue. Time-depth conversion of seismic horizons are based on a layered acoustic velocity (V_p) model and performed in S&P Global Kingdom Suite, and then the converted depth horizons were spatially interpolated using Kriging to generate continuous surfaces across the lake basin. These V_p values were derived from core-to-seismic correlations in the similar Lake Castor, located 630 km south of Lake Riñihue and near the Patagonian Andes (Van Daele et al., 2016), where similar seismic-stratigraphic units have been identified. We used 1450 m s^{-1} for Holocene sediments (e.g., Moernaut, 2010; Moernaut et al., 2018), 2200 m s^{-1} for consolidated glaciolacustrine deposits (e.g., Brückl et al., 2010; Burschil et al., 2019), 2400 m s^{-1} for till, and 3000 m s^{-1} for bedrock (Table 1), consistent with the V_p reported in previous studies (e.g., Finckh et al., 1984; Strasser et al., 2007). Alternative V_p settings, using 1450 m s^{-1} for Holocene sediments, 1800 m s^{-1} for unconsolidated glaciolacustrine deposits (e.g., Pinson et al., 2013; Ndiaye et al., 2014), 2400 m s^{-1} for till, and 3000 m s^{-1} for bedrock, are provided in the Table S1.

Shear-wave velocities (V_s) were assigned to each seismic-stratigraphic unit and constrained by empirical relationships from previous studies and shear-wave velocity data from other glacigenic lake environments. This includes the V_s-V_p relationships established by Castagna et al. (1985), Hamilton (1976), and Brocher (2005), in combination with velocity ranges from Shynkarenko et al. (2021), who performed ambient vibration analysis from Ocean Bottom Seismometer (OBS) data in glacigenic Lake Lucerne, Switzerland. As a result, each unit was assigned one of the following velocities (Table 1): Holocene lacustrine sediments were assigned V_s = 100 m s^{-1}, consistent with previously studied values (<=100 m s^{-1}) for soft lake sediments (Caiti et al., 1994; Shynkarenko et al., 2021); the glaciolacustrine unit was assigned V_s = 200 m s^{-1}, within the range (50-250 m s^{-1}) for proglacial lake deposits (Shynkarenko et al., 2021); the glacial till unit was assigned V_s = 400 m s^{-1}, within the range (200-1000 m s^{-1}) for glacial moraine (Carr et al., 1998); and the bedrock basement unit was assigned V_s = 1000 m s^{-1} in accordance with the National Earthquake Hazards Reduction Program site classification (e.g., Shynkarenko et al., 2021; Wils et al., 2026).

The time-averaged shear-wave velocity in the upper 30 meters (V_{s30}) serves as a primary proxy for site amplification in many GMPEs (Borcherdt, 1994; Wald and Allen, 2007). Based on the established geological model and shear-wave velocity ranges (Sections 3.1.1–3.1.2), we construct a V_{s30} model across Lake Riñihue. At each grid node in the model, a vertical profile of layer thicknesses (d_i) and the corresponding representative velocities (V_{si}) was extracted from the 3D velocity model. The V_{s30} value was subsequently computed using the mean shear-wave velocity for the upper 30 m of sediment beneath the lake floor as follows:

$$V_{s30} = \frac{30}{\Sigma \frac{d_i}{V_{si}}} \quad (1)$$

https://doi.org/10.5194/egusphere-2026-2493
Preprint. Discussion started: 1 June 2026

As a lake is a subaqueous environment, V_{s30} was calculated from the lake bed, and thus based on the sediment column beneath the lake floor and excluding the water layer.

3.2 Site Specific Empirical Ground Motion Prediction

Shaking intensities for the 2010 and 1960 earthquakes at Lake Riñihue were estimated using the Chile-calibrated GMPEs developed by Montalva et al. (2017) for PGA and Montalva et al. (2022) for PGV, following the general relations established by Abrahamson et al. (2016) for subduction environments:

$$PGA_{mean} \text{ or } PGV_{mean} = e^{\theta + f_{source} + f_{path} + f_{event/depth} + f_{site} + \delta Be} \quad (2)$$

where θ is the empirical coefficient of each ground motion regression; f_{source} is the magnitude scaling factors calculated based on the moment magnitude (M_w); f_{path} characterizes the geometric expansion and anelastic attenuation with rupture distance R; $f_{event/depth}$ is used to distinguish between intraslab and interface earthquakes, and as only interface earthquakes are used in this study, this term does not affect the results for either PGA or PGV; f_{site} is the site-specific term; and δB_e is an event-specific correction term representing the median difference between observed and predicted ground motions across all measured stations for the considered event. In the PGA calculation, f_{site} captures both linear and nonlinear site amplifications based on the local V_{s30}, while in the PGV calculation, it additionally includes the site's fundamental frequency (f_0).

For the 1960 earthquake, a finite-fault rupture model yields a closest distance to the rupture plane of R ≈ 63 km for Lake Riñihue (Moreno et al., 2010; Cifuentes, 1989). Although the M_w 9.5 magnitude exceeds the strict calibration range of the considered GMPEs, the models demonstrate reasonable scaling behavior for large megathrust events through its bilinear magnitude functions (Montalva et al., 2017; Montalva et al., 2022). For the 2010 M_w 8.8 Maule earthquake, the coseismic slip distribution gives an R of 132 km (Delouis et al., 2010), resulting in significantly lower ground motions compared to the 1960 earthquake. For both events, the site specific PGA and PGV were calculated by using the corresponding V_{s30} at each grid node site in the lake basin (Section 3.1.2), and the site-specific fundamental frequencies of the lake basin sediments, calculated as $f_0 = \frac{V_S}{4H}$, were used for the f_{site}, term in the PGV calculations. δB_e values are adopted from Wils et al. (2026), with −0.013 (PGA) and 0.258 (PGV) for the 2010 event, and 0 for both PGA and PGV for the 1960 event as no direct observations have been made for the 1960 earthquake. The GMPEs of Montalva et al. (2017, 2021) currently represent the most appropriate empirical ground-motion models for Chilean megathrust earthquakes, although the reported mean values are associated with large errors of σ = 0.46 for ln(PGA) and σ = 0.59 for ln(PGV) .

3.3 Numerical Modeling of Site Response

To capture complex basin amplification effects that are not fully represented in 1D site response approximations, 2D finite-elements numerical simulations of seismic wave propagation through the Lake Riñihue sedimentary basin were performed.

https://doi.org/10.5194/egusphere-2026-2493
Preprint. Discussion started: 1 June 2026

This physics-based approach accounts for vertical variations in layer properties, basin geometry effects, and wave interactions that are critical for understanding the spatial distribution of ground motion characteristics and their relationship to observed sedimentary imprints (Semblat et al., 2002; Taborda and Roten, 2015).

3.3.1 2D Numerical Modeling

Numerical simulations were established using the open-source computational platform OpenSees (Mckenna et al., 2010; Mazzoni et al., 2006) by using the pressure-independent multi-yield plasticity (PIMY) model for each unit's characteristics (Yang et al., 2003). The two-dimensional model was constructed along a seismic profile of the lake oriented east-west through its southwestern subbasin (Figure 2), parallel to the subbasin axis. As a result, the 2D numerical model consists of a 4500 m wide east-west cross-section of the lake subbasin, extending to a depth of 260 m that includes the full sedimentary sequence down to the underlying bedrock (Figure 2c).

The finite element mesh used in the 2D numerical model consists mainly of four-node quadrilateral plane-strain elements with adaptive sizing based on the local unit shear-wave velocity, balancing accuracy requirements against computational cost. Element dimensions were determined using the criterion $h \leq V_s/(8f_{max})$, where h represents model element size, V_s is the local shear-wave velocity, and f_{max} = 5 Hz was chosen to be slightly larger than f_0 to represent the maximum frequency of interest (Lysmer and Kuhlemeyer Roger, 1969). To minimize boundary effects, the numerical model was additionally extended with 1000 m on both lateral sides and 500 m beneath the basin. At the base and lateral boundaries of the model, viscous dashpots developed by Lysmer and Kuhlemeyer Roger (1969) were applied as artificial boundaries which can effectively absorb distorted reflected waves at the truncated boundary.

Bulk density values for Holocene lacustrine sediments and glaciolacustrine deposits were derived from measured core data from Lake Castor, which contains comparable glacigenic sedimentary facies and depositional conditions (Van Daele et al., 2016). The density values for glacial till and basement were assigned based on previous studies for compacted subglacial tills and bedrock (e.g., Clarke et al., 2008; Koppes et al., 2010; Mavko et al., 2009).

The nonlinear, inelastic stress-strain response of the lithological units was simulated using the PIMY constitutive model (Yang et al., 2003). The shear modulus (G) and bulk modulus (K) were directly computed from seismic velocities (V_p and V_s) using the relationships: shear modulus $G = \rho \times {V_s}^2$ and bulk modulus $K = \rho \times ({V_p}^2 - 4/3{V_s}^2)$, where ρ is bulk density. The internal friction angle of each unit used in the model was based on Wiemer et al. (2015) for a nearby glacigenic piedmont lake in south-central Chile (Lake Villarrica; 65 km north of Lake Riñihue). All layer parameters for each unit are provided in Table 1.

Table 1. Key parameters for the 2D numerical modeling

https://doi.org/10.5194/egusphere-2026-2493
Preprint. Discussion started: 1 June 2026

Layer	Geological stratum	Bulk density (g cm^{-3})	V_p (m s^{-1})	V_s (m s^{-1})	Shear modulus (Pa)	Bulk modulus (Pa)	Friction Angle (°)
Unit 3	Holocene sediments	1.2	1450	100	1.21×10^{7}	2.42×10^{9}	33
Unit 2	Glaciolacustrine deposits	1.6	2200	200	6.23×10^{7}	7.45×10^{9}	36
Unit 1	Glacial till	2.3	2400	400	3.68×10^{8}	1.18×10^{10}	40
Unit 0	Basement	2.6	3000	1000	2.60×10^{9}	1.95×10^{10}	45

To understand each unit's contribution to the local site response, we stepwise modified model properties while preserving the geometric boundaries. Seven sets of different combinations of unit parameters were used to test how different geological units contribute to ground motion amplification (Table 2, Table S2). The realistic lake basin model (BM01) represents the normal stratigraphy interpreted from seismic profiles: soft Holocene deposits (ρ=1200 kg m^{-3}, V_s=100 m s^{-1}) consecutively overlying glacio-lacustrine sediments (ρ=1600 kg m^{-3}, V_s=200 m s^{-1}), till (ρ=2300 kg m^{-3}, V_s=400 m s^{-1}), and bedrock basement (ρ=2600 kg m^{-3}, V_s=1000 m s^{-1}). BM02 assigns basement properties to the till layer (unit 2), while BM03 extends the basement properties to all pre-Holocene units (units 0-2). BM04 replaces Holocene properties (unit 3) with those of glacio-lacustrine sediments and BM05 extends the till parameter to the bedrock unit. Finally, BM06 and BM07 represent uniform property distributions using Holocene and basement parameters, respectively.

Table 2. Summary of property setting for each unit in 2D basin models. See Table S2 for detailed material parameters of each model.

Model	Unit 3 (Holocene)	Unit 2 (Glaciolacustrine)	Unit 1 (Till)	Unit 0 (Bedrock)
BM01	Holocene	Glaciolacustrine	Till	Bedrock
BM02	Holocene	Glaciolacustrine	Bedrock	Bedrock
BM03	Holocene	Bedrock	Bedrock	Bedrock
BM04	Glaciolacustrine	Glaciolacustrine	Till	Bedrock
BM05	Holocene	Glaciolacustrine	Till	Till
BM06	Holocene	Holocene	Holocene	Holocene
BM07	Bedrock	Bedrock	Bedrock	Bedrock

We also applied two sets of flat-layered reference models (FM01 and FM02) (Figure S1) with horizontal interfaces that use the same vertical stratigraphic units as those extracted from two selected locations within the basin (Figure 2c) and extend

https://doi.org/10.5194/egusphere-2026-2493
Preprint. Discussion started: 1 June 2026

them laterally across the same model length as the Basin Model. FM01 and FM02 use the same stratigraphic units and material properties as the basin models (Table 2), differing only in the relative thickness of the sedimentary sequence and the underlying bedrock. FM01 corresponds to a thinner sediment and thicker bedrock unit, while FM02 represents a thicker soft sedimentary section as is present in the central part of the basin. Each of the seven stratigraphic parameter sets were applied to both flat models, which could then directly be compared with the Basin Models to quantify amplification contributed by the 2D structure versus each of the lithological unit succession. These flat models thus mimic 1D models and allow us to test the influence of spatial variability (i.e., basin morphology and topography) on ground motion amplification, as well as to directly compare the results with GMPE-based predictions relying solely on V_{s30} (and f_0).

3.3.2 Input Motion

To select the set of acceleration waveforms to be used as input for the ground response analysis, we performed spectral matching. Reference bedrock response spectra for basement input motions were calculated from the Montalva et al. (2017) GMPEs, but with the f_{site} term removed to represent basement conditions without any site effects:

$$IM = e^{\theta + f_{source} + f_{path} + f_{event/depth} + \delta Be} \quad (3)$$

where IM represents the considered intensity measure (PGA, PGV, or spectral acceleration). The parameters used to calculate these reference spectra for both earthquakes are the same as detailed in Section 3.2. These calculated reference spectra are subsequently used as target spectra for the selection and scaling of input ground motions.

Based on these target spectra, seven sets of acceleration waveforms for each earthquake were selected from the NGA-Subduction database, which contains strong-motion recordings from subduction zone earthquakes worldwide (Bozorgnia et al., 2021), to realistically simulate the ground motions (Bommer and Acevedo, 2004; Tarbali and Bradley, 2016) that occurred in the Lake Riñihue basin basement during the 1960 M_w 9.5 Valdivia and 2010 M_w 8.8 Maule earthquakes. The selection criteria include interface event type, moment magnitudes within ± 2.0 of the target events, and recording sites with $V_{s30} > 700$ m s^{-1} to represent basement conditions. The selected motion recordings were scaled to match their respective target spectra by using scaling factors between 0.25 and 4.

These 14 selected accelerograms (Figure 3) were subsequently applied as vertical SV-waves with incidence at the base boundary nodes of the model (Figure 2c) to simulate the seismic excitation during these major earthquakes. Surface acceleration, velocity, and displacement time histories were recorded at all surface nodes across the lake basin model, providing a detailed spatial resolution of basin ground motion amplification along the profile. PGA and PGV values for each input accelerogram were calculated directly from horizontal component of time histories.

https://doi.org/10.5194/egusphere-2026-2493
Preprint. Discussion started: 1 June 2026

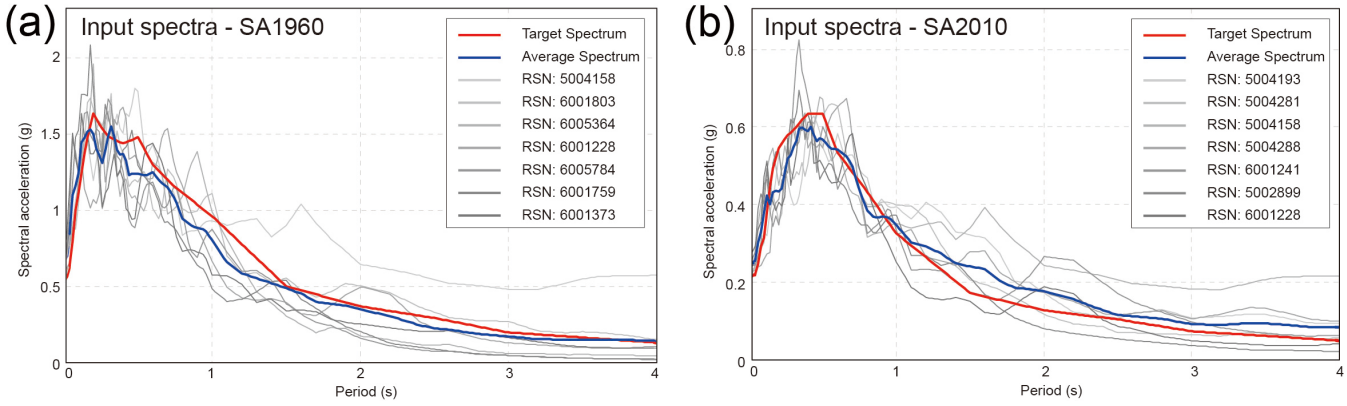

Figure 3. Input response spectra for the 2D numerical simulations. (a) Target and matched response spectra for the 1960 M_w 9.5 Valdivia earthquake scenario. (b) Target and matched response spectra for the 2010 M_w 8.8 Maule earthquake scenario. Red lines show target spectra calculated from GMPEs (Montalva et al., 2017) without site terms. Gray lines show seven ground motion records selected from the NGA-Subduction database (Bozorgnia et al., 2021), matched to interface rupture mechanisms and basement site conditions (V_{s30} >= 700 m s^{-1}). Blue lines show the average spectrum of selected records for each event.

3.4 Sedimentary Imprints and Statistical Analysis

To relate the simulated ground motions to sedimentary imprints, we compiled a dataset of existing earthquake-related sedimentary records in Lake Riñihue (Molenaar et al., 2021; Molenaar et al., 2022), and correlated those to additionally available sediment cores that were not considered in previous studies (Figure S4). We focus on two types of in-situ coseismic sedimentary imprints that directly record the local sediment response to seismic shaking: surficial sediment remobilization (SSR) and soft-sediment deformation structures (SSDS). For each core, SSR was quantified by the remobilization depth, corresponding to the thickness of stratigraphic gaps attributed to coseismic erosion of the surficial sediment drape on the hemipelagic lake slopes when comparing to the basin sedimentary sequence (Niederstätter et al (in review)). SSDS, when present, were characterized by their deformation thickness and type. Three deformation types are considered: disturbed laminations, folds, and intraclast breccia which can be related to shear-induced Kelvin–Helmholtz instability (KHI) (Molenaar et al., 2022; Molenaar et al., 2024; Lu et al., 2020; Wetzler et al., 2010). Where SSDS and stratigraphic gaps occur in conjunction, we include the remobilization depth in the SSDS thickness and identify the SSDS type solely on the preserved deformation structures in the cores. Univariate and multivariate regression analyses were applied to evaluate the influence of slope angle and ground motion parameters on sedimentary imprints (Table S3).

4 Results

4.1 V_{s30} Distribution in Lake Riñihue

Using the 3D shear-wave velocity model, we constructed a V_{s30} map across Lake Riñihue. This shows a spatial variability that is clearly controlled by the distribution of its underlying stratigraphic layers (Figure 4a): V_{s30} values range from 100 m s^{-1} in areas dominated by thick Holocene sediments, to 450 m s^{-1} where glacial till is close to the lake floor or where the total

https://doi.org/10.5194/egusphere-2026-2493
Preprint. Discussion started: 1 June 2026

sediment thickness is minimal. The western slopes show elevated V_{s30} values (200-300 m s^{-1}) due to reduced Holocene sediment thickness and proximity to the underlying till and bedrock units. In contrast, the eastern main subbasin shows markedly lower V_{s30} values (100-180 m s^{-1}), reflecting thicker soft Holocene and glaciolacustrine sediments.

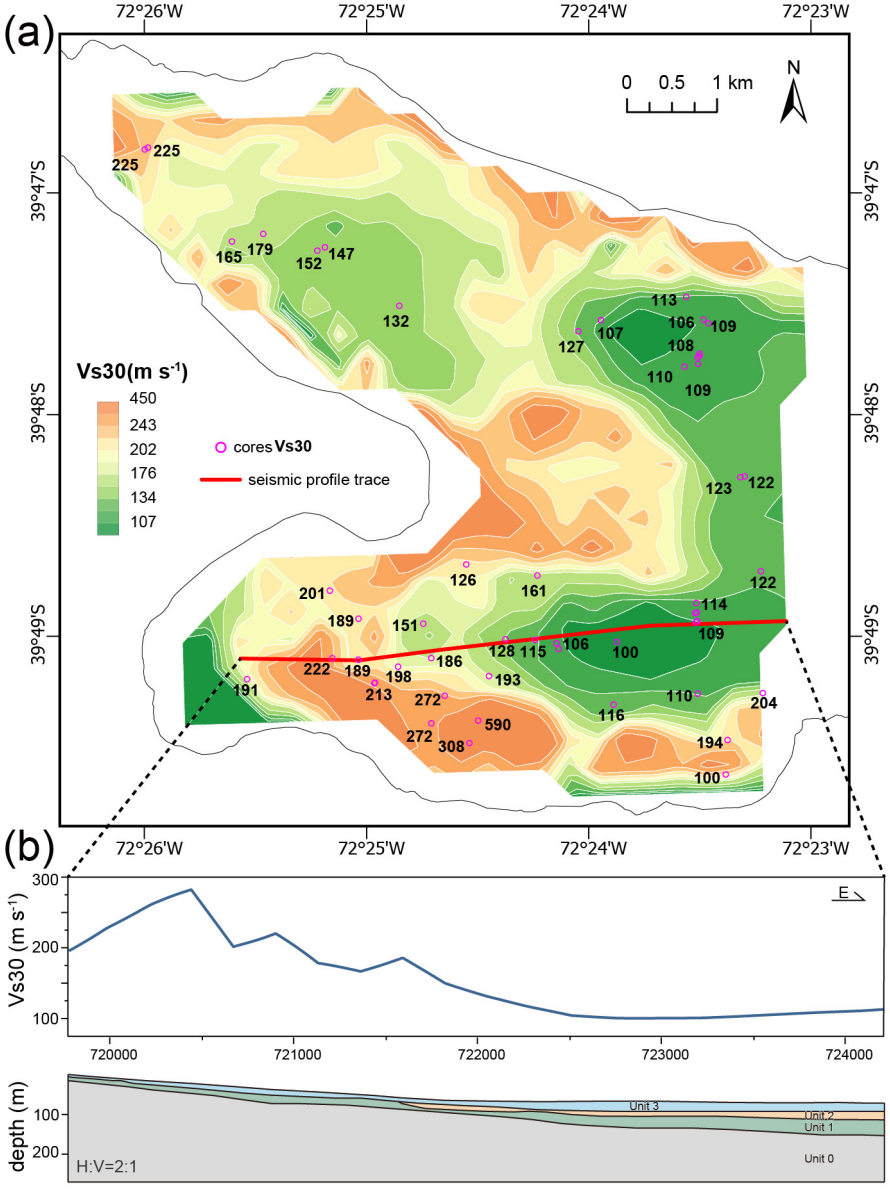

Figure 4. Spatial distribution of V_{s30} in Lake Riñihue and its variation along the seismic profile. (a) Map of V_{s30} values calculated from the 3D shear-wave velocity model. Values range from 107 m s^{-1} in areas with thick Holocene sediments to 450 m s^{-1} where glacial till is close to the lake floor. Pink circles indicate core locations with corresponding V_{s30} values. The red line indicates the seismic profile trace shown in Figure 2. (b) V_{s30} distribution along the east-west profile, showing higher values (~280 m s^{-1}) at the western area decreasing to ~110 m s^{-1} in the central basin.

https://doi.org/10.5194/egusphere-2026-2493
Preprint. Discussion started: 1 June 2026

4.2 Ground Motion Predictions from GMPEs

Ground motion predictions based on site-specific V_{s30} values using GMPEs (Montalva et al., 2017; Montalva et al., 2022) reveal several key differences between the 1960 M_w 9.5 Valdivia and 2010 M_w 8.8 Maule earthquakes (Figure 5). For the 1960 M_w 9.5 Valdivia earthquake, PGA values range from 0.24 g to 0.53 g across the entire studied subbasin, with a mean value of approximately 0.38 g (Figure 5a). The spatial distribution shows high PGA values (>0.38 g) mainly in the western parts of the study area, corresponding to regions with less soft sediment thickness and higher V_{s30} values. Correspondingly, the eastern lake subbasin shows lower PGA values (0.24-0.38 g) associated with thicker soft sediment accumulation and lower V_{s30} (Figure 4). The 2010 M_w 8.8 Maule earthquake, occurring at greater distance from the lake, produced substantially lower ground motions, and PGA values range from 0.17 g to 0.23 g (Figure 5c) suggesting approximately a 50% reduction compared to the 1960 event. However, the spatial pattern mimics that of the 1960 earthquake – albeit less pronounced, with higher values in the western part (0.21-0.23 g) and lower in the eastern lake subbasin (0.17-0.20 g), reflecting the consistent influence of local site conditions. In contrast, PGV values show an opposite spatial trend, with lower values in the western part and higher in the eastern lake subbasin for both earthquake. For the 1960 earthquake, PGV ranges from 20 cm s^{-1} to 74 cm s^{-1}, with the mean value around 47 cm s^{-1}. The high PGV values (>50 cm s^{-1}) occur in the central and eastern lake subbasin areas (Figure 5b). This spatial divergence between PGA and PGV reflects the frequency-dependent nature of site amplification, with PGV being more sensitive to longer-period ground motions (Kramer, 1996; Bommer and Alarcon, 2006) that are amplified by the presence of soft sediment (Bard and Bouchon, 1985). For the 2010 earthquake, PGV ranges from 10 cm s^{-1} to 38 cm s^{-1} with a similar spatial distribution, again at approximately half of the 1960 values (Figure 5d). These spatial variations in ground motion, with up to a 2-fold amplitude difference from west to east across the basin for both events, thus directly mimic the shallow shear-wave velocity structure that is strongly controlled by sediment thickness.

https://doi.org/10.5194/egusphere-2026-2493
Preprint. Discussion started: 1 June 2026

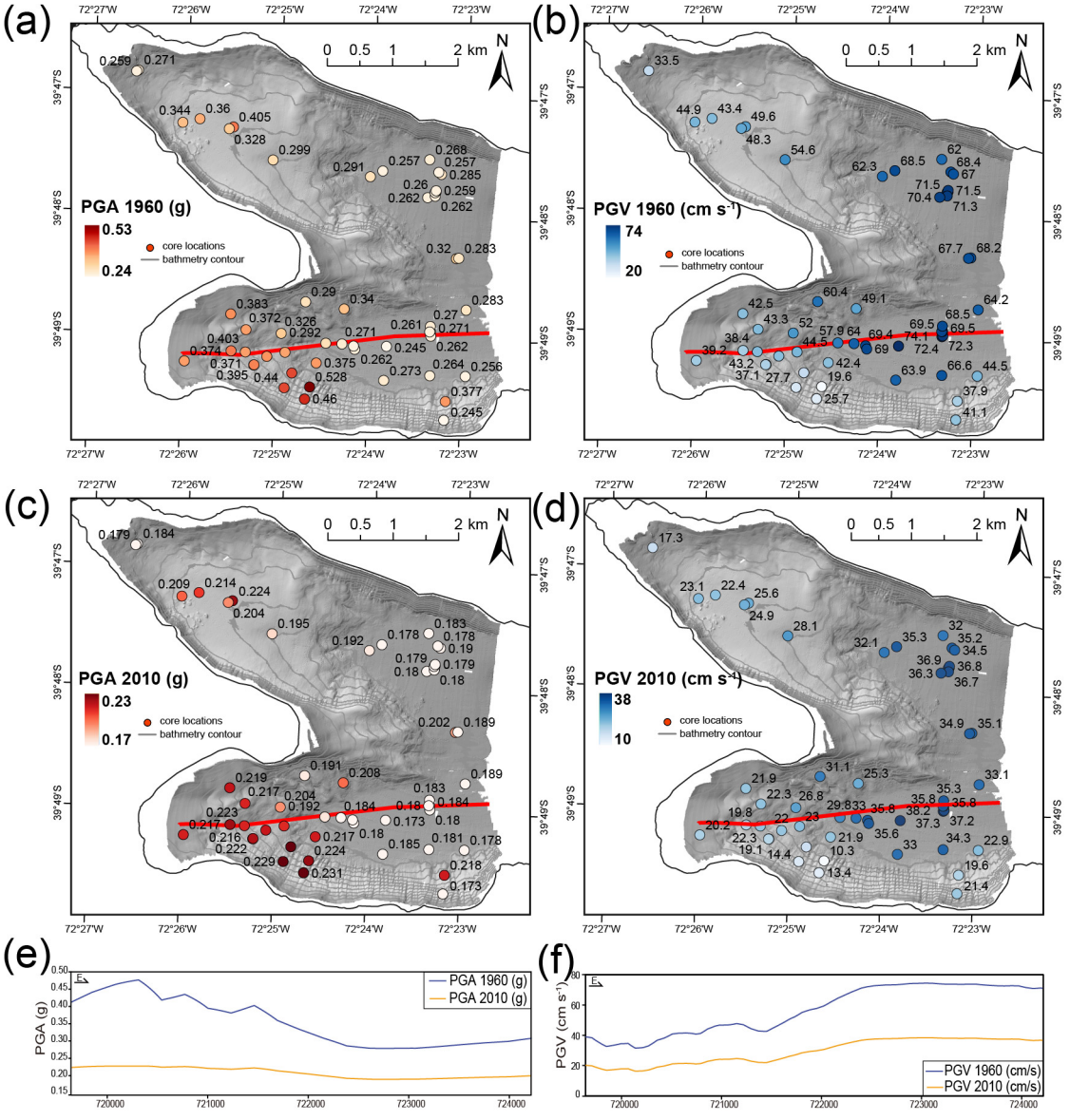

325 **Figure 5. Spatial distribution of GMPEs calculated ground motions at core locations in Lake Riñihue. (a) PGA for the 1960 M_w 9.5 Valdivia earthquake (0.24–0.53 g). (b) PGV for the 1960 earthquake (20–74 cm s^{-1}) (c) PGA for the 2010 M_w 8.8 Maule earthquake (0.17–0.23 g) (d) PGV for the 2010 earthquake (13–38 cm s^{-1}). For map views (a-d), ground motions were calculated by V_{s30} values at core locations (Figure 4a). (e) PGA along the west–east profile (red line in the map) for both earthquakes. (f) PGV values along the west–east profile for both earthquakes. (e) and (f) use V_{s30} values from the velocity model along the profile (Figure 4b). GMPEs**
330 **from Montalva et al. (2017, 2022) were used for all calculations.**

https://doi.org/10.5194/egusphere-2026-2493
Preprint. Discussion started: 1 June 2026

4.3 Ground Motions from 2D Numerical Simulations

4.3.1 Ground Motions in the Realistic Lake Basin Model

The reference basin model (BM01) uses the same stratigraphic unit structure as our original seismic interpretation with soft Holocene lacustrine sediments overlying glaciolacustrine deposits, glacial till, and bedrock (Figure 2).

Along the considered east–west profile, lake bottom surface ground motions vary considerably. PGA (Figures 6a) fluctuates heavily between 1.2 g and 1.5 g (the spread among the seven input records spans approximately 1.0 to 2.0 g) for the 1960 event in the western area, where a gradual slope is present (Figures 8). Toward the east, into the deeper central basin, PGA drops and an overall smoother and more uniform trend becomes visible. The 2010 event shows less lateral variation on its absolute value but with a similar trend, with PGA fluctuating around 0.5 g in the western area and becoming relatively stable around 0.4 g toward the subbasin in the east.

The modelled PGV (Figure 7a) shows different trends compared to the PGA. For the 1960 earthquake, it ranges from 60-110 cm s^{-1} in the western margin, with local peaks exceeding 110 cm s^{-1} at around 1.5 and 2 km basinward, and stabilizes around 80 cm s^{-1} towards the central-eastern basin. For the 2010 earthquake, PGV fluctuates between 25-50 cm s^{-1}, with similar spatial patterns but significantly lower values. Localized peaks remain evident in the western margin, yet the overall PGV amplitudes are higher in the eastern basin for both events. This indicates that basin geometry-controlled wave behavior has a more prominent impact on the relative variability of site effects for both PGA and PGV compared to input motion differences for each event.

Comparison with GMPE predictions reveals that 2D simulated ground motions are substantially higher throughout the basin (dashed lines in Figures 6a and 7a). For the 1960 earthquake, GMPEs predict PGA values of only ~0.3-0.5 g in the basin, approximately 2-2.5 times lower than 2D simulation results. The 2010 earthquake shows similar amplification scaling in the interior basin (PGA ~0.38 g vs. GMPE ~0.2 g). For PGV, both approaches result in similar values in the eastern subbasin, but at the western slope margin, 2D-simulated PGV exceeds GMPE estimates by a factor of two.

https://doi.org/10.5194/egusphere-2026-2493
Preprint. Discussion started: 1 June 2026

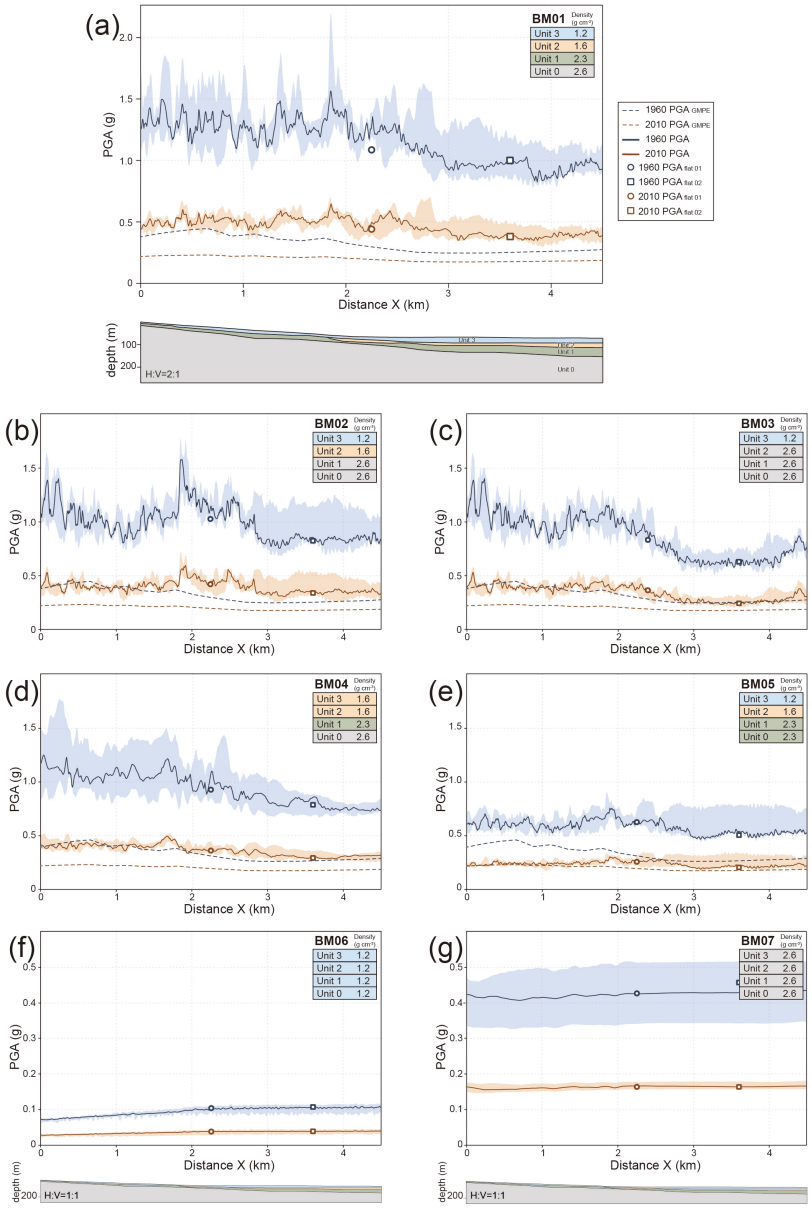

Figure 6. Along-profile peak ground acceleration (PGA) from2D numerical simulations for seven sets of basin-model parameters (a) BM01 with realistic stratigraphy. (b–e) Models with progressively stiffer deeper units. (f–g) Uniform end-member models with Holocene and bedrock properties, respectively. Dashed lines show the profile PGA results from GMPEs. Solid lines show median PGA for the 1960 (blue) and 2010 (orange) earthquakes; shaded envelopes span the range across seven input motions for each event. Dashed lines indicate GMPE predictions. Circles and squares indicate PGA from flat-layered reference models FM01 and FM02, respectively. Depth-converted cross-sections are shown beneath (a), (f), and (g).

https://doi.org/10.5194/egusphere-2026-2493
Preprint. Discussion started: 1 June 2026

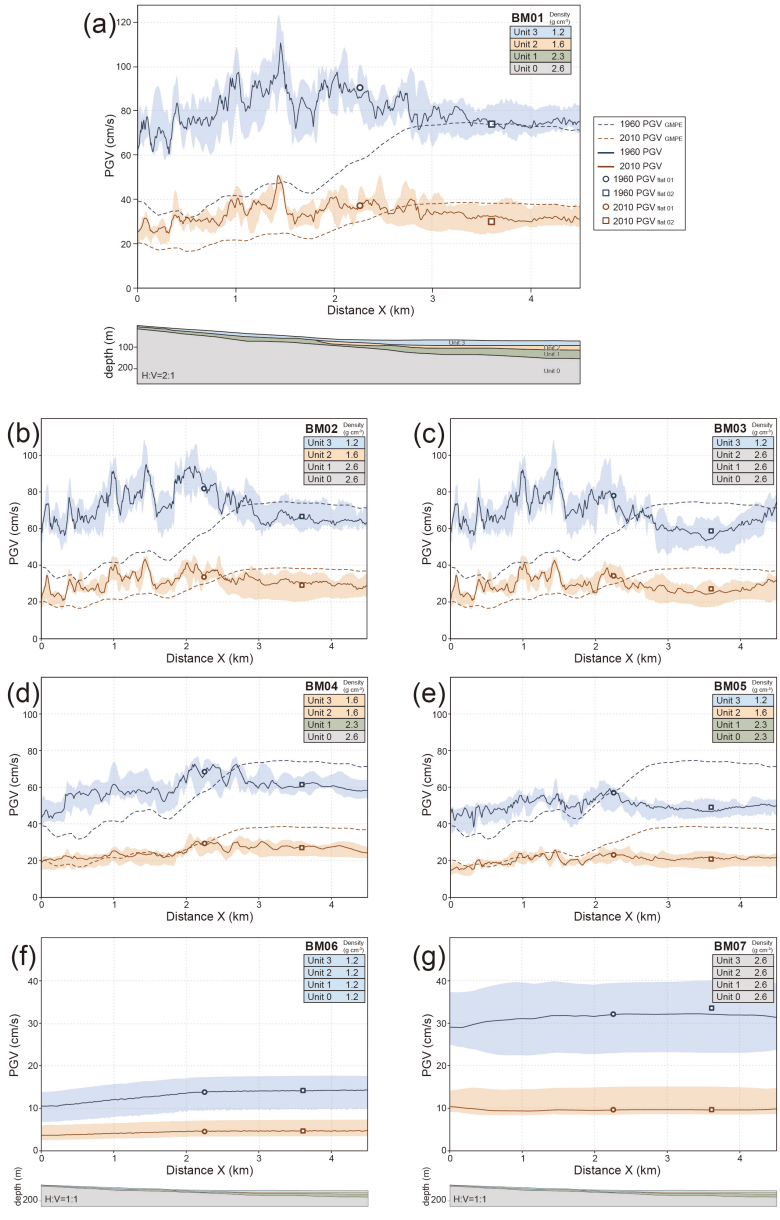

Figure 7. Along-profile peak ground velocity (PGV) from2D numerical simulations for seven sets of basin-model parameters (a) BM01 with realistic stratigraphy. (b–e) Models with progressively stiffer deeper units. (f–g) Uniform end-member models with Holocene and bedrock properties, respectively. Dashed lines show the profile PGV results from GMPEs. Solid lines show median PGV for the 1960 (blue) and 2010 (orange) earthquakes; shaded envelopes span the range across seven input motions for each event. Dashed lines indicate GMPE predictions. Circles and squares indicate PGV from flat-layered reference models FM01 and FM02, respectively. Depth-converted cross-sections are shown beneath (a), (f), and (g).

https://doi.org/10.5194/egusphere-2026-2493
Preprint. Discussion started: 1 June 2026

4.3.2 Influence of Basin Stratigraphy and Morphology

To evaluate the influence of different stratigraphic units on local ground motion strength, we tested six additional basin models (BMs 02–07) that share the same geometric boundaries as the actual lake stratigraphy but differ in their material properties (Table 2). Four of the models (BMs 02–05) produce ground motions that exceed the GMPE predictions and show a similar spatial distribution (Figures 6-7) as those of the realistic model (BM01). However, the highest ground motions among all BMs are still achieved by BM01. Despite their differences in unit properties, each model shows higher PGA toward the west, with multiple localized peaks resulting from the subbasin geometry (Figures 2b-c), and gradually lower and more uniform amplitudes toward the east (Figures 6a-e). PGV systematically shows the opposite trend with lower values at the western margin and higher values in the eastern basin (Figures 7a-e), although several local peaks along the slope interrupt this overall pattern. In contrast, the two end-member models (BM06 and BM07), which assume uniform material properties throughout the basin, show reduced lateral variability and lower PGA and PGV (Figures 6f-g and 7f-g) compared to all other basin models.

BM02 (Figures 6b and 7b), with bedrock properties assigned to both unit 0 and unit 1, slightly reduces ground motions relative to BM01, but the PGA and PGV spatial trends along the east–west profile still persist. Removing the intermediate-velocity till layer stiffens the lower unit column, thus slightly decreasing overall ground motion amplification. The soft Holocene and glaciolacustrine layers still result in lower PGA, but only marginally higher PGV in the eastern basin compared to the western slopes. Indeed, the local peaks on the slopes become more prominent for both PGA and PGV.

BM03 (Figures 6c and 7c) further decreases ground motions but keeps the overall PGA and PGV spatial trends as in the realistic BM01. With only a thin unit of soft Holocene sediment covering the stiff basement, amplification is even less than in BM02, yet PGA and PGV further show more prominent localized peaks on the slopes, suggesting a strong control of the low-velocity Unit 3 on these local peaks, and especially the contrast with overlying units. This shows that even simplified two-unit models can result in basin-wide spatial variations controlled by sediment thickness variations.

BM04 (Figures 6d and 7d), without the soft Holocene cover, leads to less amplification compared to BMs 01-03 as removing the softest layer reduces the wave impedance contrast at the surface. However, the remaining glaciolacustrine sediments still provide enough velocity contrast to generate notable amplification. Both PGA and PGV show smoother spatial variations, and their overall trends become more similar to the GMPE predictions, although its absolute amplitudes are still increased.

BM05 (Figures 6e and 7e), in which the basement is replaced by till properties, leads to a further reduction in ground motion strength compared to the above-described models. Nevertheless, the spatial pattern with higher PGA in the east and lower in the west still remains, indicating that the unit properties continue to influence ground motion distributions, even when the lower unit shear-wave velocity contrasts are slightly diminished.

https://doi.org/10.5194/egusphere-2026-2493
Preprint. Discussion started: 1 June 2026

The two uniform models (BMs 06 and 07) (Figures 6f, 6g, 7f and 7g) are simulated to distinguish the effects of basin geometry from the stratigraphic effect, and result in markedly lower ground motion intensities. BM06 (Figures 6f and 7f), with entirely soft Holocene units, results in large attenuation of both PGA and PGV, with values decreasing to ~0.1 g and ~10 cm s^{-1} for 1960 event, respectively. Despite the uniform model properties, PGA and PGV both show a subtle increasing trend from the western margin, where the total sediment thickness is smaller, toward the central subbasin, where it is greater. However, ground motion values for BM07 (Figures 6f and 7f) (a uniform bedrock model) closely follow the input motions (Figure 3), with minimal spatial variation across the profile, and the simulated PGA and PGV values (~0.46 g and ~32 cm s^{-1} for the 1960 event; ~0.17 g and ~10 cm s^{-1} for the 2010 event) are consistent with previous GMPE-based estimates for bedrock (Wils et al., 2026).

The flat-layer reference models (FM01 and FM02) result in PGA and PGV values that fall within the range of the basin model simulations (Figures 6-7). FM02, which represents the thicker sedimentary sequence of the central subbasin, produces weaker ground motions than FM01, which corresponds to the thinner sedimentary cover at the basin margin. However, all flat models generate uniform ground motions across the profile and do not reproduce the localized PGA or PGV peaks in the western margin (Figures S5-S8).

4.4 Sedimentary imprints

4.4.1 Sediment cores

The collected and reanalyzed CT data of 19 sediment cores are distributed across the southwestern subbasin of Lake Riñihue and reveal spatially variable earthquake-induced sedimentary imprints associated with the 1960 M_w 9.5 Valdivia earthquake (Molenaar et al., 2022; Molenaar et al., 2021). The 2010 M_w 8.8 Maule earthquake did not produce identifiable SSR or SSDS in any of the studied cores.

SSR attributed to coseismic surficial remobilization during the 1960 event are present in nearly all cores in the margin, but vary in depth from ~1 cm (e.g., RIN17-07, RIN17-09) to ~20 cm (e.g., RIN17-01, RIN17-02) (Figure S4). The largest gaps are concentrated along the western basin slope where slope angles are highest (Figures 8a-b), whereas cores from the flatter subbasin areas in the east generally exhibit thinner gaps or none. SSDS also show considerable spatial variability in both thickness and deformation type. Deformation thicknesses range from ~1 cm (e.g., RIN17-18) to ~25 cm (e.g., RIN17-09), and deformation types include disturbed laminations (e.g., RIN17-03) (Figure 8d) and folds (e.g., RIN17-05) (Figure 8c). We do not observe intraclast breccia related to the 1960 earthquake in any of the cores.

A visual comparison between SSR (stratigraphic gaps) depths and SSDS thicknesses across our core dataset suggests that these two types of seismic imprints are not directly related. Several locations (e.g. RIN17-01, RIN17-18) display large

https://doi.org/10.5194/egusphere-2026-2493
Preprint. Discussion started: 1 June 2026

surficial remobilization but only very thin SSDS or none, whereas other sites contain clearly developed thick SSDS but show only minimal remobilization (e.g. RIN17-11).

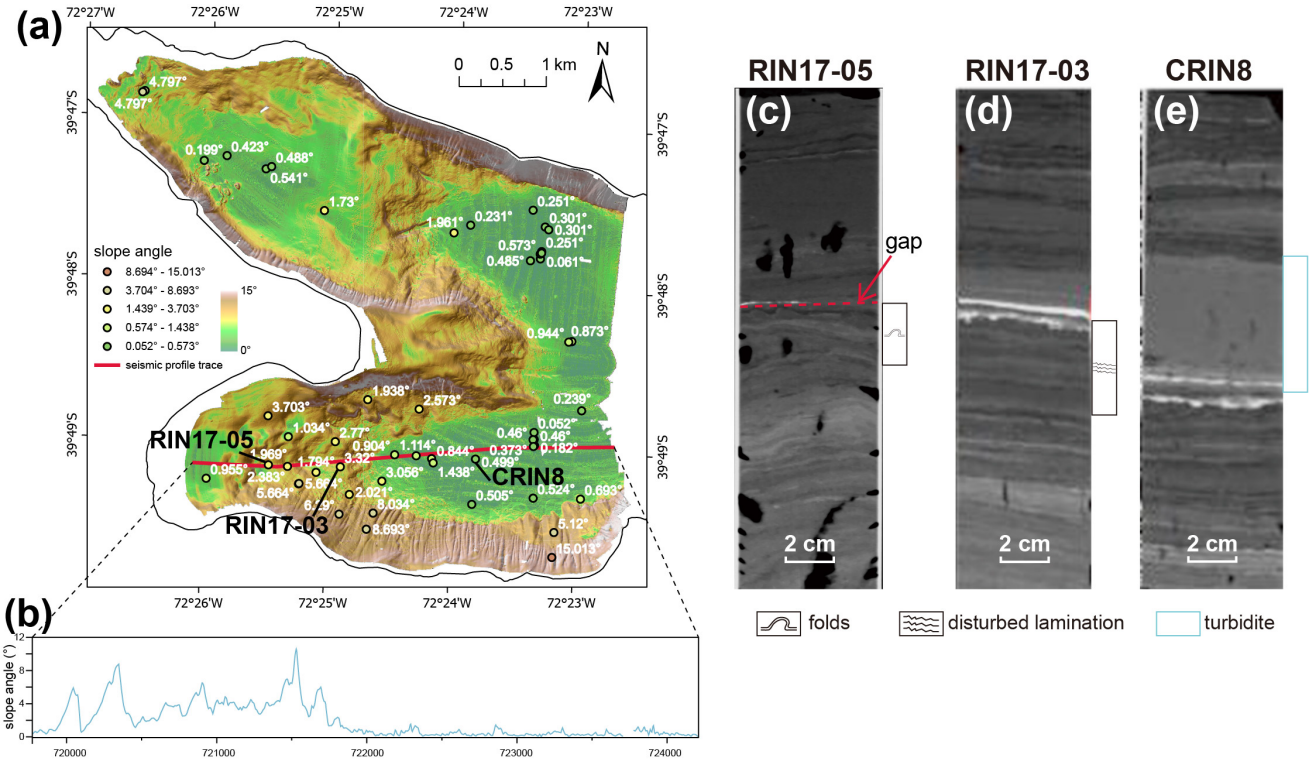

Figure 8. Slope angle distribution and representative sedimentary imprints in Lake Riñihue. (a) Slope angle map calculated from high-resolution bathymetry. Circles indicate core locations with corresponding slope angle values. (b) Slope angle along the east-west profile, showing the contrast between the rugged topography in the western areas and the flat lake floor to the east. (c–e) CT scan images examples from sediment cores (Figure S4) showing sedimentary imprints attributed to the 1960 M_w 9.5 Valdivia earthquake: (c) RIN17-05 with folds and SSR; (d) RIN17-03 with disturbed laminations; (e) CRIN8 is a reference core without SSR or SSDS.

4.4.2 SSR depth and SSDS thickness versus ground motions

All sedimentary imprints used for statistical analysis are attributed to the 1960 M_w 9.5 Valdivia earthquake as the 2010 M_w 8.8 Maule earthquake did not leave a visible evidence (SSR nor SSDS) in the studied cores. Therefore, the 2010 event is used only for qualitative comparisons of minimum ground motions thresholds. Univariate and multivariate regressions for SSR depth (Figures S9–S10) and SSDS thickness (Figures S11–S13) were performed using slope angle, PGA, and PGV derived from both GMPE predictions and 2D simulations.

Among univariate regressions considering SSR depth, slope angle is the strongest single predictor (R^2 = 0.85; Table S3). However, multivariate regressions combining slope angle with PGV produce the highest R^2 values across all tested

https://doi.org/10.5194/egusphere-2026-2493
Preprint. Discussion started: 1 June 2026

regressions, reaching 0.90–0.94 for GMPE-based estimates and 0.91–0.93 for 2D simulation results (Figure S10), with consistently positive PGV coefficients across all functional forms. In contrast, regressions combining slope angle with PGA yield negative PGA coefficients regardless of whether GMPE or 2D-simulated values are used (Figure S9), and R^2 values do not improve systematically over slope-angle-only models (Figure 9). Among these, the regression ln(SSR) = f(slope, ln(PGV)) yields the best fit (R^2 = 0.94 for GMPE-based PGV) (Figure S10c), suggesting a nonlinear scaling between SSR depth and PGV.

Given that only five cores with SSDS are located adjacent to the seismic profile, we complemented this small subset with regressions using all cores in the basin that contain SSDS related to the studied event and for which ground motions were calculated using GMPEs. In univariate regressions of SSDS thickness, PGA is the strongest single predictor, but still with limited R^2 (R^2 = 0.33, for the logarithm) (Figure S11h), while slope angle alone (R^2 = 0.12) and PGV alone (R^2 = 0.29, also with negative coefficient) (Figure S11c) produce poorer correlations. Multivariate regressions combining PGA with slope angle have the highest R^2 among all SSDS regressions, reaching 0.47 (linear) (Figure S12a) and 0.48 (logarithm) (Figure S12e), with positive PGA coefficients in both fits. Regressions combining PGV with slope angle have lower R^2 (0.29–0.46) (Figure S13), with negative PGV coefficients in all functional forms. Overall, all SSDS regressions ($R^2 \leq 0.48$) explain substantially less variance in the observed data than SSR regressions (R^2 up to 0.94) (Figure 9).

https://doi.org/10.5194/egusphere-2026-2493
Preprint. Discussion started: 1 June 2026

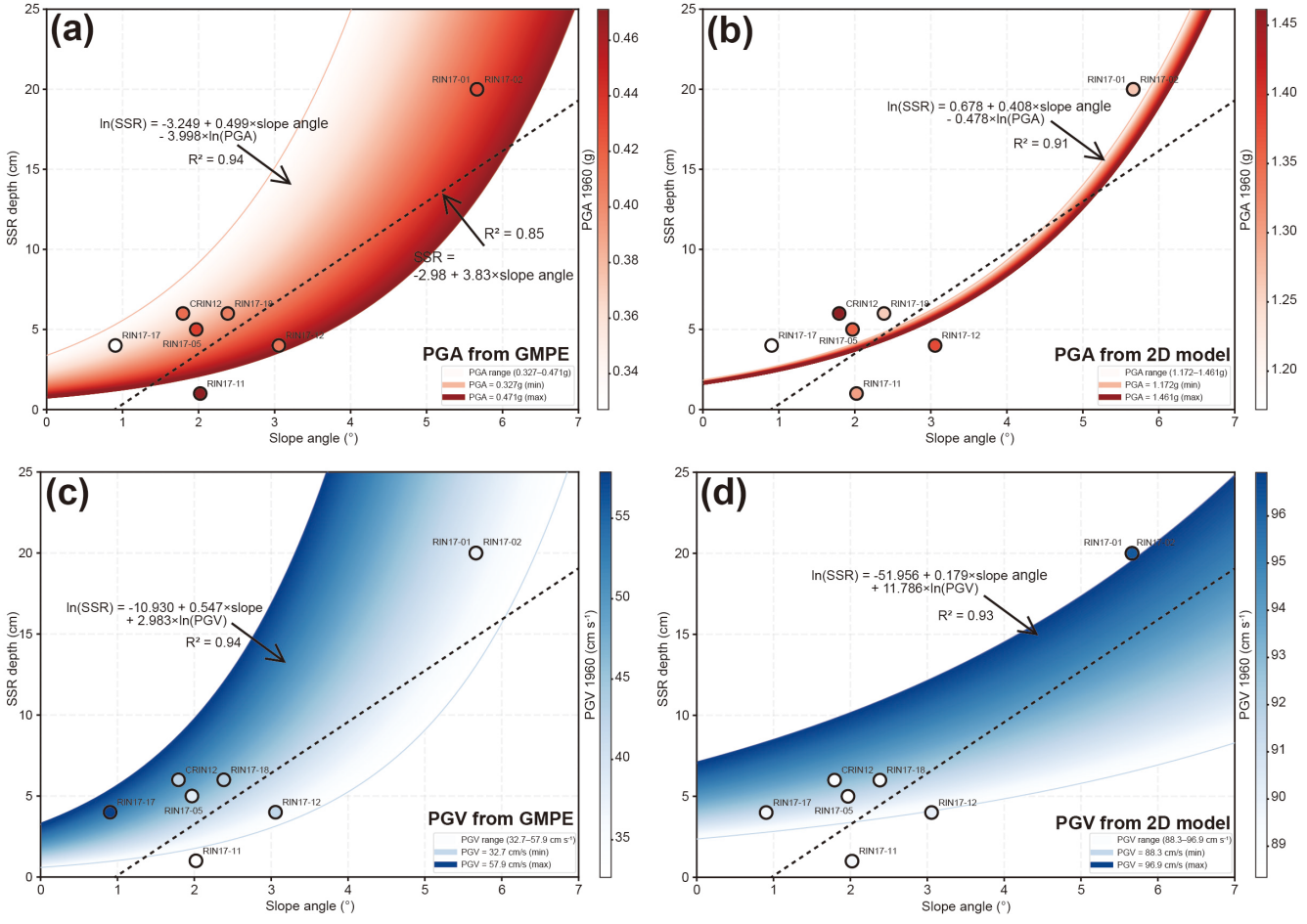

Figure 9. Multivariate regressions of surficial sediment remobilization (SSR) thickness against slope angle and ground motion parameters for the 1960 M_w 9.5 Valdivia earthquake. (a–b) SSR depth versus slope angle colored by PGA from (a) GMPE predictions and (b) 2D simulations. (c–d) SSR depth versus slope angle colored by PGV from (c) GMPE predictions and (d) 2D simulations. Dashed lines show the univariate reference regression for SSR and slope angle. Color gradients represent PGA (red) (a–b) and PGV (blue) (c–d) ranges across core locations.

5 Discussion

5.1 Stratigraphic Control on Ground Motion Amplification in Lake Riñihue

The GMPE-based prediction using spatially variable V_{s30} values provides an initial view of site-specific ground motion distribution across the studied lake basin (Figures 4-5), with higher PGA but lower PGV in areas with stiffer units (V_{s30} values of 200–275 m s^{-1} along the western margins), and lower PGA but higher PGV within the softer sediments (V_{s30} values of 100–150 m s^{-1} in the eastern subbasin). The spatially variable V_{s30} (Figure 4) (and f_0) distribution thus leads to corresponding variations in GMPE-predicted ground motions across the studied basin (Figure 5). As such, it allows rapid basin-wide computations, providing a significant improvement for comparisons of local ground motions with sedimentary

https://doi.org/10.5194/egusphere-2026-2493
Preprint. Discussion started: 1 June 2026

imprints observed in sediment cores with respect to using a single value for the entire lake basin (e.g., Wils et al., 2026; Molenaar et al., 2024; Moernaut et al., 2014; Avşar et al., 2016). However, these GMPE calculations based on spatially variable V_{s30} (and f_0) values cannot fully capture the amplifications predicted by 2D numerical simulations (Figures 6a and 7a).

The 2D numerical simulations show ground motion amplifications in Lake Riñihue that exceed GMPE-based predictions by a factor 2 for both the 1960 M_w 9.5 Valdivia and 2010 M_w 8.8 Maule earthquakes (Figures 6-7). We infer that part of these amplification differences reflect the lack of consideration of the subsurface structure in GMPEs, as these mainly rely on V_{s30} (and f_0) variations as the single proxy for site amplification term (Castellaro et al., 2008; Pitilakis et al., 2013; Stewart et al., 2014). As GMPEs are developed and calibrated primarily using terrestrial strong-motion stations (e.g., Montalva et al., 2017; Montalva et al., 2022), with only a limited number of stations occupying the lowest V_{s30} range (100 m s^{-1}), lake basins filled with very soft Holocene sediments are not represented by this calibration dataset. Although we calculated V_{s30} for the sediment units beneath the lake floor, the low-density, high-porosity, diatomaceous nature of the lacustrine sediments in Lake Riñihue differs from the terrestrial soil sites used. Despite exhibiting relatively high static shear strength, diatomaceous sediments are susceptible to induce excess pore water pressure and potential liquefaction under cyclic seismic loading (Wiemer and Kopf, 2017; Wiemer et al., 2017). These properties suggest that lake sediments may require lake basin-specific GMPE calibrations to more realistically represent their seismic response characteristics.

While V_{s30} provides a simple and practical parameter for engineering applications, it represents a simplification of the actual subsurface conditions. GMPEs do not explicitly incorporate the full velocity structure, impedance contrasts between layers, or basin geometry, all of which could influence seismic wave propagation and ground motion amplification in a lake basin (e.g., Borcherdt, 1994; Wald and Allen, 2007). Such basin effects include: (1) geometric focusing of seismic waves due to basin shape and irregular interface topography; (2) generation of surface waves where impedance contrasts are pronounced; (3) lateral propagation of these surface waves through the basin interior; (4) constructive and destructive interference between incident body waves and basin-generated surface waves; and (5) two-dimensional and/or three-dimensional resonance related to basin scales (Bard and Bouchon, 1985; Chávez-García et al., 1996; Semblat et al., 2002; Parla and Somala, 2022). For example, the high impedance contrasts in Lake Riñihue, with soft Holocene lacustrine sediments (V_s = 100 m s^{-1}) overlying successively stiffer glaciolacustrine deposits (V_s = 200 m s^{-1}), glacial till (V_s = 400 m s^{-1}), and bedrock (V_s = 1000 m s^{-1}), create impedance ratios of 5 to 10 that can generate efficient wave trapping and resonance within the sedimentary units (Table 1) (Caiti et al., 1994; Shynkarenko et al., 2021; Carr et al., 1998). Such multi-layered structure with strong impedance contrasts at different depths cannot be adequately represented by only a single V_{s30} value.

The 2D numerical simulations of the basin models and flat models with unique unit parameters (Table 2) (Figures 6-7) provide further insights into how vertical stratigraphic characteristics indeed influence seismic ground motion in lake basins. The results from the uniform “end-member” models (BM06, BM07, FM01-6, FM01-7, FM02-6 and FM02-7) underscore

https://doi.org/10.5194/egusphere-2026-2493
Preprint. Discussion started: 1 June 2026

that some amplification preconditions could be overlooked in simplified analyses (Figures 6f-g, 7f-g, Figures S5f-g, Figures S6f-g, Figures S7f-g and Figures S8f-g). BM07, as well as FM01-7 and FM02-7, with uniform basement properties, reproduces the basement input and shows negligible site amplification, owing to the absence of internal impedance contrasts in stiff bedrock units. In contrast, BM06, FM01-6 and FM02-6, with uniform soft Holocene properties, shows substantial attenuation rather than amplification, with surface ground motions much lower than input motions. This attenuation reflects the lack of impedance contrasts and lateral units variation that are needed to trap and focus seismic energy within the basin (Bard and Bouchon, 1985; Roten et al., 2006); instead, incident waves propagate through the thick, uniformly soft Holocene units, where their energy dissipates through material damping and geometric spreading (Bard and Bouchon, 1985; Richards and Menke, 1983). This result cautions against the common intuition that "softer" means "more amplified ground motions" in lake basin settings. Thus, the overall ~2-fold amplification in 2D simulation relative to GMPEs primarily results from the different lithological units and spatial basin geometry rather than V_{s30} alone.

By gradually replacing deeper stratigraphic units with bedrock properties across BM01 to BM03 (also in flat models) ground motion amplification decreases (Figures 6a-c and 7a-c). This reduction shows that ground motion amplification scales with the stacking of distinct units, such as Holocene over glaciolacustrine sediment, over till, or over bedrock, rather than with the averaged properties of the upper tens of meters as considered in a V_{s30} value. This cumulative effect of impedance contrasts at multiple stratigraphic boundaries is further supported by BM05, where removing the deepest bedrock contrast substantially reduces ground motion amplification despite retaining all sedimentary units, and by BM06, where removing all internal impedance contrasts results in ground motion attenuation rather than amplification. Moreover, the comparison between BM01 and BM04 (Figures 6a,d and 7a,d) also highlights the importance of the surficial Holocene unit, as replacing only this uppermost unit with glaciolacustrine properties reduces the overall amplification by 30–40% and suppresses localized peak values along the western slopes. This influence of surficial soft Holocene sediment on the overall amplification and strong lateral variability is consistent with site response observations in other soft-sediment environments, where strong impedance contrasts at shallow depths dominate seismic amplifications (Borcherdt, 1994; Kramer, 1996; Ayoubi et al., 2021).

5.2 Lateral Variability in Ground Motion Intensity Controlled by Basin Morphology

Beyond overall ground motion amplification, our 2D simulations show spatial asymmetry in ground motions from west to east over the lake basin (Figures 6-7). The western slope shows localized spikes occurring over 2 km, while the eastern basin area shows lower and more uniform amplitudes (Figure 6a). The lateral trends in PGA and PGV (Figures 6-7) persist in both the 1960 and 2010 earthquakes and across all basin models with the same geometry but varying unit properties (BMs 01–05). In contrast, the flat models (Figures S5–S8) with the same unit properties produce similar overall amplification levels but lack the pronounced west–east asymmetry and localized peak values shown in the basin models.

https://doi.org/10.5194/egusphere-2026-2493
Preprint. Discussion started: 1 June 2026

Indeed, the western part of the study area consists of several confined depressions that act as small sub-basins (Figure 2), with lateral dimensions ranging from hundreds of meters to a few kilometers. These spatial scales are comparable to the wavelengths of the dominant input seismic frequencies (Figure 3), allowing these individual sub-basins to selectively amplify different frequency components. Similar small-scale basin resonance has been reported in other complex basins, where localized impedance contrasts and irregular topography produce distinct spectral peaks and amplifications (Raptakis et al., 2005). This wavelength-dependent interaction means that different frequency components experience varying degrees of constructive and destructive interference as they propagate through the basin (Makra et al., 2005; Semblat et al., 2005). The result is rapid spatial variations in ground motion amplitude, with many PGA and PGV spikes concentrated in the western area of the basin (Figures 6-7). In contrast, the eastern area has more flat and thicker sediments, supporting lower-frequency and long-period wave propagation that increases PGV and duration rather than PGA (Roten et al., 2006; Boore and Atkinson, 2008) (Figures 6-7). This indicates that basin morphology primarily controls the lateral variability of ground motion, whereas lithological contrasts influence the overall amplification level. As a result, the interaction among lithological contrasts, basin geometry and earthquake frequency content controls which parts of a lake basin experiences the strongest effective shaking. Large-magnitude earthquakes, rich in low-frequency energy, are thus expected to preferentially amplify motion within deeper, laterally continuous basin interiors, whereas earthquakes with relatively higher-frequency content may more effectively excite short-wavelength amplification at confined sub-basins. These sub-basin effects could provide a physical explanation for the strong spatial variability of SSDS and SSR observed between earthquakes, as well as during a single event (e.g., Molenaar et al., 2021).

5.3 From Ground Motion Parameters to Sedimentary Records

5.3.1 Linking Ground Motion to Surficial Sediment Remobilization

We applied multivariate regressions to evaluate the influence of slope angle (Figure 8) and/or ground motion parameters (PGA, PGV) on surficial sediment remobilization (SSR) depth (Figure 9 and Figures S9-10). These regressions using both GMPE predictions and 2D simulation results consistently identify slope angle as the primary control, which has the lowest p-value (0.001) among all tested parameters (Table S3). This is consistent with previous studies in Chilean lakes, where remobilization depth and gap occurrence increase with slope angle (Molenaar et al., 2021). The strong slope angle control reflects the important role of gravitational instability: steeper slopes experience larger downslope shear stress components, reducing the seismic forcing required to overcome sediment shear strength and initiate downslope remobilization (e.g., Shen et al., 2025; Molenaar et al., 2021). Similar enhanced sensitivity of steeper slopes to earthquake-induced remobilization has been reported in Alpine and other lacustrine settings, where gravitational downslope stress brings deposits closer to failure so that only modest additional dynamic loading is required to trigger erosion or sliding (Wilhelm et al., 2016; Strasser et al., 2007).

https://doi.org/10.5194/egusphere-2026-2493
Preprint. Discussion started: 1 June 2026

However, the multivariate regressions incorporating both slope angle and ground motion parameters - whether from GMPE-based estimates or 2D simulated results (R^2 = 0.87-0.94) - provide improved statistical fits to SSR depth compared to slope angle alone (R^2 = 0.85) (Figure 9, Figure S9 and Figure S10), suggesting that, expectedly, ground motions also contribute to SSR depth. Although multivariate regressions including PGA improve the statistical fit compared to slope angle alone, the obtained negative PGA regression coefficients (Figures 9a-b Figure S9) indicate that PGA is not a physically meaningful predictor of sediment gap thickness. PGA mainly reflects high-frequency shaking and instantaneous acceleration peaks (Kramer, 1996), which are inefficient in driving cumulative sediment stripping (e.g., Jibson, 2007; Kramer and Mitchell, 2006) and may therefore fail to capture the mechanisms for SSR.

In contrast, the multivariate regressions including PGV show a positive and physically consistent contribution of ground motion, with regressions combining slope angle and PGV providing the best statistical fits to SSR depth (R^2 = 0.94 for GMPE-based estimates and R^2 = 0.93 for the 2D simulations) (Figures 9c-d and Figure S10). This is consistent with recent work from many south-central Chile lakes, showing that surficial sediment remobilization and related seismoturbidite presence are well correlated with PGV (Wils et al., 2026). Notably, we also observe stratigraphic gaps on very gentle slopes, such as in core RIN17-17 where the local slope angle is < 1°. However, this site experienced the highest PGV among all core locations, indicating that slope angle acts as a preconditioning factor, but sufficiently high PGV values could independently initiate surficial remobilization in areas with minimal gravitational forcing. Field and experimental studies also demonstrate that even small increases in slope angle can largely enhance susceptibility to remobilization and deformation, while very steep slopes may cease to accumulate thick drapes of fine sediment, limiting the preservation of earthquake imprints (e.g., Niederstätter et al (in review); Molenaar et al., 2024; Molenaar et al., 2021; Wiemer et al., 2015; Seibert et al., 2025). We therefore infer that slope angle and PGV jointly control surficial remobilization. The critical slope angle required for SSR decreases with increasing PGV, whereas higher PGV are needed to trigger SSR on gentler slopes.

The good correlation between remobilization and PGV could reflect the physical mechanism by which seismic shaking remobilizes surficial lake sediments. Wils et al. (2026) proposed that surficial remobilization relies on a velocity contrast between the moving sedimentary substrate and the static overlying water column, resulting in shear stress at the sediment-water interface that progressively overcomes sediment cohesion (Figure 11a). As PGV particularly reflects longer-period and low-frequency components (Kramer, 1996; Molenaar et al., 2021), this remobilization mechanism, initiating at the sediment-water interface through seismically-induced transient stresses (Gomberg, 2018; Moernaut et al., 2017), has been validated by physical experiments showing that shear between sediment and water during low-frequency ground motion can entrain several centimeters of surficial sediment (e.g., Seibert et al., 2025).

The spatial distribution of SSR-related gaps is patchy, as observed in sediment cores by Molenaar et al. (2021) as well as in this study. The 2D simulations show that PGV varies substantially across the basin for the 1960 earthquake, with pronounced lateral trends and localized amplification peaks (Figure 7a). Because SSR depends on both local slope angle and PGV, and

https://doi.org/10.5194/egusphere-2026-2493
Preprint. Discussion started: 1 June 2026

these two factors vary independently, where slope angle is influenced by basin morphology and PGV is influenced by stratigraphic layering and basin geometry, SSR is distributed heterogeneously rather than uniformly across the basin. This is supported by the core evidence: for example, RIN17-17 in a flatter area with a moderate slope angle but higher PGV shows ~4 cm SSR depth, whereas RIN17-12 on a steeper slope with lower PGV also exhibits ~4 cm (Figures 9 and S4). This spatial heterogeneity is consistent with observations by Molenaar et al. (2021), who reported that the distribution of stratigraphic gaps varies between different paleoseismic events (e.g., 1575, 1837, 1906 CE) at the same core sites in Lake Riñihue. Because basin geometry and slope angles remain essentially constant over these timescales, the variable gap depths between events indicate that differences in earthquake source characteristics, such as frequency content, rupture directivity, and shaking duration, produce different PGV distributions across the basin, thereby causing remobilization on different slopes. Therefore, even large earthquakes are unlikely to remobilize all susceptible slopes simultaneously, allowing for the preservation of continuous lacustrine paleoseismic records.

5.3.2 Linking Ground Motion to SSDS Deformation

Previous multi-lake studies have shown that stratigraphic variability, specifically lithology and physical properties of deforming sediments, is one of the primary factors controlling SSDS deformation (e.g., Heifetz et al., 2005; Molenaar et al., 2022; Molenaar et al., 2024; Wetzler et al., 2010). Sediment composition influences shear strength and susceptibility to deformation: diatom-rich sediments exhibit higher particle interlocking and surface roughness, which increases resistance to shear-induced deformation compared to clastic or organic-rich facies (Molenaar et al., 2024). Volcanic deposits interbedded within lacustrine sequences can further modulate SSDS occurrence by providing potential dewatering surfaces that facilitate deformation during subsequent seismic events (Molenaar et al., 2021). In the present study, however, we focus on SSDS resulting from a single event (i.e. 1960 earthquake) in Lake Riñihue, so that the laterally uniform lithology removes stratigraphic variability as a primary control on SSDS formation (Niederstätter et al (in review)).

Our regression analyses (Section 4.4.2, Table S3) consistently identify PGA as a ground motion parameter controlling SSDS. Among all tested ground motion parameters, PGA yields the strongest positive correlation with SSDS thickness and type, whereas PGV shows a weaker and negative correlation (Figures S11-S13). These results are consistent with previous finding by Molenaar et al. (2021) reporting that SSDS type correlates best with PGA across six megathrust earthquakes, providing field-based evidence of progressive SSDS development with increasing PGA for deformation caused by Kelvin–Helmholtz instability (KHI) (Figure 11b). Indeed, ground acceleration amplitude directly influences the Richardson number at layer interfaces by generating velocity differentials between adjacent layers of different densities (Heifetz et al., 2005; Wetzler et al., 2010). Higher PGA reduces the effective Richardson number below the critical threshold for instability onset, causing gradually more intense deformation from disturbed laminations through folds to intraclast breccia (Lu et al., 2020). In contrast to PGA, PGV does not provide any reasonable thresholds for SSDS type in our study. The 2D simulations show overlapping PGV ranges among deformation types (Figure 10e). Apparent PGV thresholds in the GMPE estimations

https://doi.org/10.5194/egusphere-2026-2493
Preprint. Discussion started: 1 June 2026

(Figures 10a–b) are artifacts of the inverse trend between PGA and PGV with respect to V_{s30}, which produces a spurious pattern where stronger deformation coincides with lower PGV, opposite to what would be physically expected for increased KHI (e.g., Wils et al., 2026; Lu et al., 2020).

The combined regression of PGA and slope angle provides the highest R^2 (0.48) among all SSDS regressions (Table S3). Slope angle modulates the relationship between PGA and SSDS in different ways. Notably, some sites with steep slope angles (e.g. RIN17-09, RIN17-10 and RIN17-19) have relatively thin SSDS despite high PGAs, while the thickest SSDS in the dataset occurs at core RIN17-11 on a gentle slope where PGA is relative low. Those sites could reflect slope-controlled sediment consolidation. On steeper slopes in lakes and shallow marine environments, more frequent sediment remobilization and lower net accumulation rates tend to generate a thinner and more condensed Holocene sedimentary cover with steeper compaction gradients and therefore higher shear strength (e.g., Niederstätter et al (in review); Moernaut et al., 2025; Sawyer and Devore, 2015). Under such conditions, earthquake induced shear is less likely to propagate downward, which can restrict SSDS formation even where PGA is high.

Nevertheless, all SSDS regressions provide much lower R^2 (less than 0.48) compared to SSR depth regressions (R^2 up to 0.94), likely reflecting the intrinsically heterogeneous nature of SSDS. This is because SSDS thickness not only depends on deformation intensity but also on deformation type, forming a continuum from disturbed laminations through folds to intraclast breccia rather than discrete categories. Moreover, a thinner SSDS may actually record a higher degree of deformation (e.g., Heifetz et al., 2005; Lu et al., 2020). Additionally, the subdivision into specific SSDS types represents a simplification, thus SSDS thickness parameter alone likely does not fully capture deformation intensity, and can thus not be directly linked to a specific ground motion parameter. Despite the limited regression power of ground motion intensity for SSDS thickness, both the GMPE estimations and 2D simulations show distinct PGA thresholds for the presence of different SSDS types (Figures 10a, d and Figures S11-13). The absence of identifiable SSDS occupy the lower PGA range (< 0.3 g), disturbed laminations appear at intermediate values (0.3 – 0.4 g), and folds at the highest PGAs (> 0.4 g). This is in line with numerical models that established a series of increasing minimum acceleration thresholds from disturbed laminations, folds, to intraclast breccia in Dead Sea Basin (Lu et al., 2020; Wetzler et al., 2010), reflecting increasing deformation intensity driven by earthquake-induced shear processes at sediment layer interfaces. In conclusion, our result suggest that in a uniform stratum, PGA acts as both the threshold parameter for SSDS type and a predictor of deformation thickness.

https://doi.org/10.5194/egusphere-2026-2493
Preprint. Discussion started: 1 June 2026

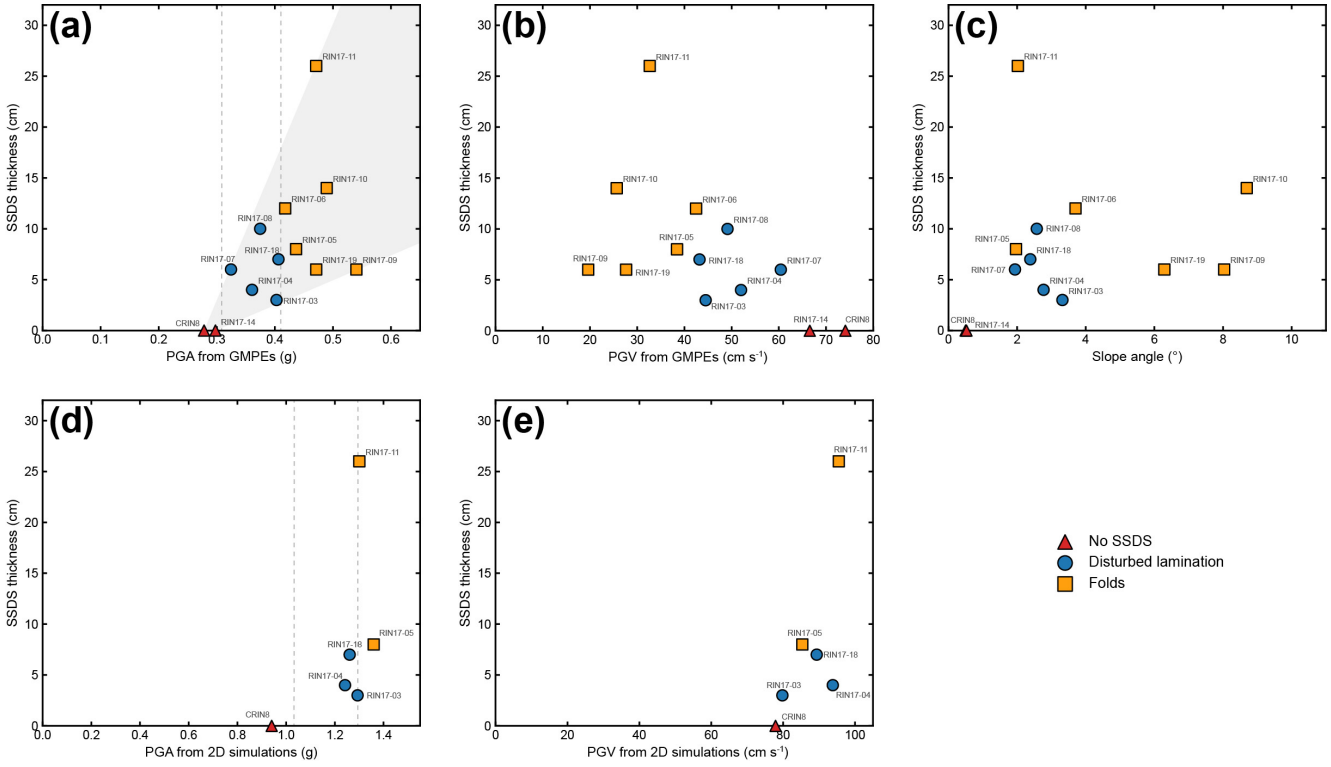

Figure 10. Relationships between SSDS thickness and ground motion parameters from GMPEs and 2D numerical simulations. (a) SSDS thickness versus GMPE-derived PGA. Gray shading marks the range of PGA values occurring at core locations, and dashed lines indicate visually identified divisions in the data distribution. (b) SSDS thickness versus GMPE-derived PGV. (c) SSDS thickness versus local slope angle; the dashed line marks the lowest slope angle at which SSDS occur in the dataset. (d) SSDS thickness versus PGA from 2D site response simulations for cores close to the model profile. (e) SSDS thickness versus PGV from 2D simulations for the same cores.

5.4 Implications for paleoseismology

Our results suggest that SSR and SSDS are two independent sedimentary processes that are controlled by different components of seismic ground motion (Figure 11). This distinction reflects fundamentally different physical mechanisms. SSDS formation through KHI requires differential motion between stratified layers, which arises from acceleration and creating shear in the sediment layers' interface (Heifetz et al., 2005), whereas at constant velocity no differential displacement develops. In contrast, SSR initiates at the sediment–water interface and reflects erosion and downslope remobilization of a surficial sediment veneer, a process that is more closely linked to velocity-driven shear at the boundary and to the duration over which that shear is sustained. Because SSR and SSDS respond to different ground motion components, they may record different aspects of past earthquakes. SSDS type primarily reflects PGA and thus high-frequency shaking intensity, whereas SSR depth and occurrence are controlled by PGV and longer-period motion (e.g. Molenaar et al., 2021; Wils et al., 2026). Together, these two types of imprints could help distinguish between earthquakes of different magnitude, distance, or frequency content, as each source type produces a characteristic ratio of PGA to PGV.

https://doi.org/10.5194/egusphere-2026-2493
Preprint. Discussion started: 1 June 2026

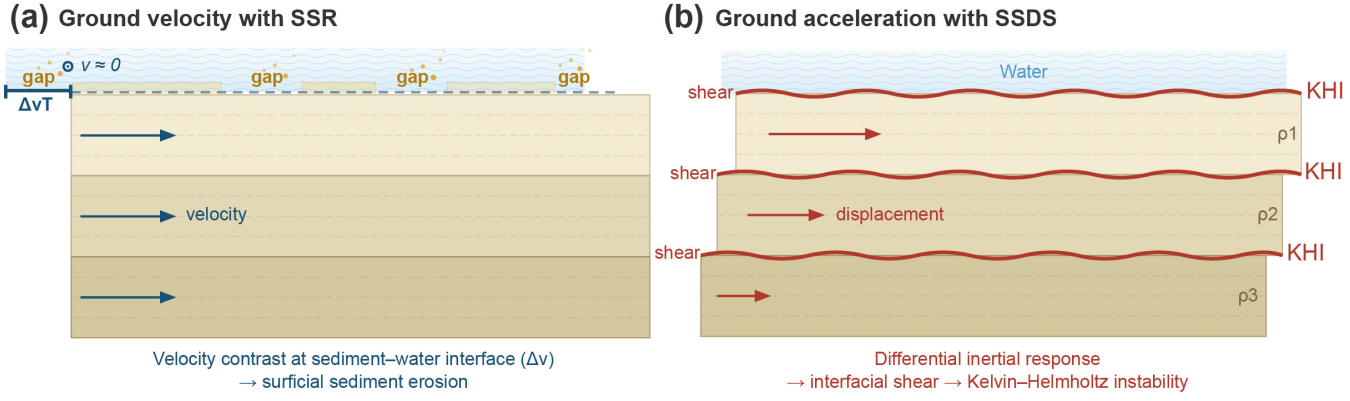

Figure 11. Conceptual models for the distinct mechanisms controlling surficial sediment remobilization (SSR) and soft-sediment deformation structure (SSDS). (a) SSR initiate at the sediment–water interface, where velocity-related motion leads to boundary shear and remove surficial sediment veneer. (b) SSDS form within the different layers' interface, where ground acceleration leads to differential inertial response between mechanically contrasting layers, producing interfacial shear and KHI-related deformation.

The sedimentary imprint is not controlled by ground motion alone, which limits the application of our approach to long sedimentary records. SSDS and SSR remain influenced by many additional factors such as slope angle, grain size, and sediment properties including grain interlocking of which the influence is not yet fully understood. As a result, the same PGA or PGV may produce different sedimentary responses in different lakes, or even at different sites within the same basin. Therefore, although the distinction between SSDS and SSR with respect to earthquake ground motion parameters provides a useful basis for interpreting lacustrine paleoseismic records, applying it to reconstruct ground motions from long sedimentary sequences requires further calibration in lakes with different lithologies, sediment properties, and basin geometry.

6 Conclusion

This study presents the first application of 2D numerical site response modeling to evaluate ground motion amplification in a lacustrine basin and its relationship to earthquake-triggered sedimentary imprints. By combining high-resolution seismic stratigraphy, empirical estimations and physics-based numerical simulations with a systematic analysis of sedimentary records from Lake Riñihue, Chile, we assess how lake basin structure modifies earthquake shaking and how this modified shaking is recorded by surficial sediment remobilization (SSR) and soft-sediment deformation structures (SSDS).

Our 2D simulations predict lake ground motions exceeding empirical GMPE estimates by a factor of two for both the 1960 M_w 9.5 Valdivia and 2010 M_w 8.8 Maule earthquakes, because GMPEs rely on V_{s30} as a simplified site proxy that does not capture the full vertical velocity and basin geometry that influences surface ground motion in lacustrine settings. Indeed, the multi-layered stratigraphy of Lake Riñihue creates high wave impedance contrast that generate efficient wave trapping and resonance. Moreover, multi-scale basin geometry effects produce obvious spatial differences in ground motion across the

https://doi.org/10.5194/egusphere-2026-2493
Preprint. Discussion started: 1 June 2026

lake. The western margin with sub-basin structures shows localized PGA spikes exceeding 1.5 g over lateral distances of hundreds of meters, while the deeper eastern basin shows more uniform and lower amplitude responses, which cannot be captured by 1D site response estimations.

The presence and thickness of SSR and SSDS do not correlate across core sites, which indicates that SSR and SSDS formation are two independent sedimentary response processes controlled by different components of ground motion during earthquakes. By comparing local ground motions to coseismic sedimentary signatures, we find that SSR is a patchy process controlled by slope angle and PGV. This result is consistent with the physical mechanism whereby the role of longer-period ground motion and shaking duration in remobilizing surficial sediments through interface shear is crucial. On the other hand, SSDS exhibit distinct PGA thresholds corresponding to increasing deformation intensity, from disturbed laminations to folds, consistent with Kelvin-Helmholtz instability. PGA acts as both the threshold parameter for SSDS type and a predictor of SSDS thickness.

Code and data availability

All data required to reproduce the results presented in this research can be found in this work and in the supplement. The code for GMPE estimations is available at https://doi.org/10.1785/0120160221 (Montalva et al., 2017) and at https://doi.org/10.1785/0120210037 (Montalva et al., 2022). The 2D numerical models based on OpenSees (Mckenna et al., 2010; Mazzoni et al., 2006) are archived in Zenodo (Yang, 2026).

Author contributions

Conceptualization: HY, KW, AM, JM, LW, MVD. Data curation: HY, KW, AM, JM, LW, RU, MP, MVD. Methodology: HY, KW, MVD. Writing – original draft preparation: HY. Writing – review & editing: HY, KW, AM, JM, LW, RU, MP, MVD. Funding acquisition: KW, JM.

Competing interests

The authors declare that they have no conflict of interest.

Acknowledgements

The authors acknowledge the financial support of the Research Foundation – Flanders and the Austrian Science Fund.

https://doi.org/10.5194/egusphere-2026-2493
Preprint. Discussion started: 1 June 2026

Financial support

This research has been supported by the Research Foundation – Flanders (FWO) [12ZC422N] and the Austrian Science Fund (FWF) [10.55776/P34504].

References

Abrahamson, N., Gregor, N., and Addo, K.: BC Hydro Ground Motion Prediction Equations for Subduction Earthquakes, Earthquake Spectra, 32, 23-44, https://doi.org/10.1193/051712EQS188MR, 2016.

Astroza, M. and Lazo, R.: Estudio de los daños de los terremotos del 21 y 22 de mayo de 1960, 2008.

Avşar, U., Jónsson, S., Avşar, Ö., and Schmidt, S.: Earthquake-induced soft-sediment deformations and seismically amplified erosion rates recorded in varved sediments of Köyceğiz Lake (SW Turkey), Journal of Geophysical Research: Solid Earth, 121, 4767-4779, https://doi.org/10.1002/2016JB012820, 2016.

Ayoubi, P., Mohammadi, K., and Asimaki, D.: A systematic analysis of basin effects on surface ground motion, Soil Dynamics and Earthquake Engineering, 141, 2021.

Bard, P.-Y. and Bouchon, M.: The two-dimensional resonance of sediment-filled valleys, Bulletin of the Seismological Society of America, 75, 519-541, https://doi.org/10.1785/BSSA0750020519, 1985.

Bommer, J. J. and Acevedo, A. B.: THE USE OF REAL EARTHQUAKE ACCELEROGRAMS AS INPUT TO DYNAMIC ANALYSIS, Journal of Earthquake Engineering, 8, 43-91, https://doi.org/10.1080/13632460409350521, 2004.

Bommer, J. J. and Alarcon, J. E.: THE PREDICTION AND USE OF PEAK GROUND VELOCITY, Journal of Earthquake Engineering, 10, 1-31, https://doi.org/10.1080/13632460609350586, 2006.

Boore, D. M. and Atkinson, G. M.: Ground-Motion Prediction Equations for the Average Horizontal Component of PGA, PGV, and 5%-Damped PSA at Spectral Periods between 0.01 s and 10.0 s, Earthquake Spectra, 24, 99-138, https://doi.org/10.1193/1.2830434, 2008.

Borcherdt, R. D.: Estimates of Site-Dependent Response Spectra for Design (Methodology and Justification), Earthquake Spectra, 10, 617-653, https://doi.org/10.1193/1.1585791, 1994.

Bozorgnia, Y., Abrahamson, N. A., Ahdi, S. K., Ancheta, T. D., Atik, L. A., Archuleta, R. J., Atkinson, G. M., Boore, D. M., Campbell, K. W., S-J Chiou, B., Contreras, V., Darragh, R. B., Derakhshan, S., Donahue, J. L., Gregor, N., Gulerce, Z., Idriss, I., Ji, C., Kishida, T., Kottke, A. R., Kuehn, N., Kwak, D., O-L Kwok, A., Lin, P., Macedo, J., Mazzoni, S., Midorikawa, S., Muin, S., Parker, G. A., Rezaeian, S., Si, H., Silva, W. J., Stewart, J. P., Walling, M., Wooddell, K., and Youngs, R. R.: NGA-Subduction research program, Earthquake Spectra, 38, 783-798, https://doi.org/10.1177/87552930211056081, 2021.

Brocher, T. M.: Compressional and shear wave velocity versus depth in the San Francisco Bay area, California: Rules for USGS Bay Area Velocity Model 05.0.0, Report 2005-1317, https://pubs.usgs.gov/publication/ofr20051317, 2005.

Brückl, E., Brückl, J., Chwatal, W., and Ullrich, C.: Deep alpine valleys: examples of geophysical explorations in Austria, Swiss Journal of Geosciences, 103, 329-344, https://doi.org/10.1007/s00015-010-0045-x, 2010.

Burschil, T., Tanner, D. C., Reitner, J. M., Buness, H., and Gabriel, G.: Unravelling the shape and stratigraphy of a glacially-overdeepened valley with reflection seismic: the Lienz Basin (Austria), Swiss Journal of Geosciences, 112, 341-355, https://doi.org/10.1007/s00015-019-00339-0, 2019.

Caiti, A., Akal, T., and Stoll, R. D.: Estimation of shear wave velocity in shallow marine sediments, IEEE Journal of Oceanic Engineering, 19, 58-72, 1994.

Campos, H.: Limnological study of Araucanian lakes (Chile), SIL Proceedings, 1922-2010, 22, 1319-1327, https://doi.org/10.1080/03680770.1983.11897493, 1984.

Carr, B. J., Hajnal, Z., and Prugger, A.: Shear-wave studies in glacial till, Geophysics, 63, 1273-1284, https://doi.org/10.1190/1.1444429, 1998.

Castagna, J. P., Batzle, M. L., and Eastwood, R. L.: Relationships between compressional-wave and shear-wave velocities in clastic silicate rocks, Geophysics, 50, 571-581, https://doi.org/10.1190/1.1441933, 1985.

Castellaro, S., Mulargia, F., and Rossi, P. L.: Vs30: Proxy for Seismic Amplification?, Seismological Research Letters, 79, 540-543, https://doi.org/10.1785/gssrl.79.4.540, 2008.

https://doi.org/10.5194/egusphere-2026-2493
Preprint. Discussion started: 1 June 2026

Chávez-García, F. J., Sánchez, L. R., and Hatzfeld, D.: Topographic site effects and HVSR. A comparison between observations and theory, Bulletin of the Seismological Society of America, 86, 1559-1573, https://doi.org/10.1785/BSSA0860051559, 1996.

Cifuentes, I. L.: The 1960 Chilean earthquakes, Journal of Geophysical Research: Solid Earth, 94, 665-680, https://doi.org/10.1029/JB094iB01p00665, 1989.

Clarke, B. G., Hughes, D. B., and Hashemi, S.: Physical characteristics of subglacial tills, Géotechnique, 58, 67-76, https://doi.org/10.1680/geot.2008.58.1.67, 2008.

Daxer, C., Huang, J.-J. S., Weginger, S., Hilbe, M., Strasser, M., and Moernaut, J.: Validation of seismic hazard curves using a calibrated 14 ka lacustrine record in the Eastern Alps, Austria, Scientific Reports, 12, 19943, https://doi.org/10.1038/s41598-022-24487-w, 2022.

Delouis, B., Nocquet, J.-M., and Vallée, M.: Slip distribution of the February 27, 2010 Mw = 8.8 Maule Earthquake, central Chile, from static and high-rate GPS, InSAR, and broadband teleseismic data, Geophysical Research Letters, 37, https://doi.org/10.1029/2010GL043899, 2010.

DeMets, C., Gordon, R. G., and Argus, D. F.: Geologically current plate motions, Geophysical Journal International, 181, 1-80, https://doi.org/10.1111/j.1365-246X.2009.04491.x, 2010.

Finckh, P., Kelts, K., and Lambert, A.: Seismic stratigraphy and bedrock forms in perialpine lakes, GSA Bulletin, 95, 1118-1128, https://doi.org/10.1130/0016-7606(1984)95<1118:SSABFI>2.0.CO;2, 1984.

Gastineau, R., Sabatier, P., Fabbri, S. C., Anselmetti, F. S., Roeser, P., Findling, N., Şahin, M., Gündüz, S., Arnaud, F., Franz, S. O., Ünsal, N. D., and de Sigoyer, J.: Lateral variations in the signature of earthquake-generated deposits in Lake Iznik, NW Turkey, The Depositional Record, 10, 470-495, https://doi.org/10.1002/dep2.232, 2024.

Gomberg, J.: Cascadia Onshore-Offshore Site Response, Submarine Sediment Mobilization, and Earthquake Recurrence, Journal of Geophysical Research: Solid Earth, 123, 1381-1404, https://doi.org/10.1002/2017JB014985, 2018.

Hamilton, E. L.: Shear-wave velocity versus depth in marine sediments; a review, Geophysics, 41, 985-996, https://doi.org/10.1190/1.1440676, 1976.

Heifetz, E., Agnon, A., and Marco, S.: Soft sediment deformation by Kelvin Helmholtz Instability: A case from Dead Sea earthquakes, Earth and Planetary Science Letters, 236, 497-504, https://www.sciencedirect.com/science/article/pii/S0012821X05002487, 2005.

Heirman, K.: 'A wind of change': changes in position and intensity of the southern hemisphere westerlies during oxygen isotope stages 3, 2 and 1, http://hdl.handle.net/1854/LU-1900377, 2011.

Howarth, J. D., Fitzsimons, S. J., Norris, R. J., and Jacobsen, G. E.: Lake sediments record high intensity shaking that provides insight into the location and rupture length of large earthquakes on the Alpine Fault, New Zealand, Earth and Planetary Science Letters, 403, 340-351, https://www.sciencedirect.com/science/article/pii/S0012821X14004580, 2014.

Howarth, J. D., Barth, N. C., Fitzsimons, S. J., Richards-Dinger, K., Clark, K. J., Biasi, G. P., Cochran, U. A., Langridge, R. M., Berryman, K. R., and Sutherland, R.: Spatiotemporal clustering of great earthquakes on a transform fault controlled by geometry, Nature Geoscience, 14, 314-320, https://doi.org/10.1038/s41561-021-00721-4, 2021.

Jibson, R. W.: Regression models for estimating coseismic landslide displacement, Engineering Geology, 91, 209-218, https://www.sciencedirect.com/science/article/pii/S0013795207000300, 2007.

Koppes, M., Sylwester, R., Rivera, A., and Hallet, B.: Variations in sediment yield over the advance and retreat of a calving glacier, Laguna San Rafael, North Patagonian Icefield, Quaternary Research, 73, 84-95, https://www.sciencedirect.com/science/article/pii/S0033589409000854, 2010.

Kramer, S. L.: Geotechnical Earthquake Engineering, 1996.

Kramer, S. L. and Mitchell, R. A.: Ground Motion Intensity Measures for Liquefaction Hazard Evaluation, Earthquake Spectra, 22, 413-438, https://doi.org/10.1193/1.2194970, 2006.

Kremer, K., Wirth, S. B., Reusch, A., Fäh, D., Bellwald, B., Anselmetti, F. S., Girardclos, S., and Strasser, M.: Lake-sediment based paleoseismology: Limitations and perspectives from the Swiss Alps, Quaternary Science Reviews, 168, 1-18, https://www.sciencedirect.com/science/article/pii/S0277379117303542, 2017.

Lemot, F., Sabatier, P., Chevalier, M.-L., Develle, A.-L., Fang, Z., Rioual, P., Zhang, S., Bai, M., Wang, S., Li, H., and Replumaz, A.: Building a Multilake Paleoseismometer for the Xianshuihe Fault (Tibetan Plateau, China), Tectonics, 43, e2024TC008508, https://doi.org/10.1029/2024TC008508, 2024.

https://doi.org/10.5194/egusphere-2026-2493
Preprint. Discussion started: 1 June 2026

Lomnitz, C.: Major Earthquakes of Chile: A Historical Survey, 1535-1960, Seismological Research Letters, 75, 368-378, https://doi.org/10.1785/gssrl.75.3.368, 2004.
Lu, Y., Wetzler, N., Waldmann, N., Agnon, A., Biasi, G. P., and Marco, S.: A 220,000-year-long continuous large earthquake record on a slow-slipping plate boundary, Science Advances, 6, eaba4170, https://doi.org/10.1126/sciadv.aba4170, 2020.
Lysmer, J. and Kuhlemeyer Roger, L.: Finite Dynamic Model for Infinite Media, Journal of the Engineering Mechanics Division, 95, 859-877, https://doi.org/10.1061/JMCEA3.0001144, 1969.
Makra, K., Chávez-García, F. J., Raptakis, D., and Pitilakis, K.: Parametric analysis of the seismic response of a 2D sedimentary valley: implications for code implementations of complex site effects, Soil Dynamics and Earthquake Engineering, 25, 303-315, https://www.sciencedirect.com/science/article/pii/S0267726105000163, 2005.
Mavko, G., Mukerji, T., and Dvorkin, J.: The Rock Physics Handbook: Tools for Seismic Analysis of Porous Media, 2, Cambridge University Press, Cambridge, https://www.cambridge.org/core/product/A53F53ADFDD5D72EF01A9E4C6E9454A7, 2009.
Mazzoni, S., McKenna, F., Scott, M. H., and Fenves, G. L.: OpenSees Command Language Manual, University of California, Berkeley2006.
McKenna, F., Scott Michael, H., and Fenves Gregory, L.: Nonlinear Finite-Element Analysis Software Architecture Using Object Composition, Journal of Computing in Civil Engineering, 24, 95-107, https://doi.org/10.1061/(ASCE)CP.1943-5487.0000002, 2010.
Meunier, P., Hovius, N., and Haines, A. J.: Regional patterns of earthquake-triggered landslides and their relation to ground motion, Geophysical Research Letters, 34, https://doi.org/10.1029/2007GL031337, 2007.
Moernaut, J.: Sublacustrine landslide processes and their paleoseismological significance: revealing the recurrence rate of giant earthquakes in South-Central Chile, Ghent University. Faculty of Sciences, http://hdl.handle.net/1854/LU-941021, 2010.
Moernaut, J. and De Batist, M.: Frontal emplacement and mobility of sublacustrine landslides: Results from morphometric and seismostratigraphic analysis, Marine Geology, 285, 29-45, https://www.sciencedirect.com/science/article/pii/S0025322711001071, 2011.
Moernaut, J., Howarth, J., Kremer, K., and Wils, K.: Lacustrine Records of Past Seismic Shaking, in: Understanding Past Earthquakes, edited by: Elliott, A., and Gruetzner, C., Springer Nature Switzerland, Cham, 169-227, https://doi.org/10.1007/978-3-031-73580-6_7, 2025.
Moernaut, J., De Batist, M., Heirman, K., Van Daele, M., Pino, M., Brümmer, R., and Urrutia, R.: Fluidization of buried mass-wasting deposits in lake sediments and its relevance for paleoseismology: Results from a reflection seismic study of lakes Villarrica and Calafquén (South-Central Chile), Sedimentary Geology, 213, 121-135, https://www.sciencedirect.com/science/article/pii/S0037073808002492, 2009.
Moernaut, J., Daele, M. V., Heirman, K., Fontijn, K., Strasser, M., Pino, M., Urrutia, R., and De Batist, M.: Lacustrine turbidites as a tool for quantitative earthquake reconstruction: New evidence for a variable rupture mode in south central Chile, Journal of Geophysical Research: Solid Earth, 119, 1607-1633, https://doi.org/10.1002/2013JB010738, 2014.
Moernaut, J., Van Daele, M., Fontijn, K., Heirman, K., Kempf, P., Pino, M., Valdebenito, G., Urrutia, R., Strasser, M., and De Batist, M.: Larger earthquakes recur more periodically: New insights in the megathrust earthquake cycle from lacustrine turbidite records in south-central Chile, Earth and Planetary Science Letters, 481, 9-19, https://www.sciencedirect.com/science/article/pii/S0012821X17305757, 2018.
Moernaut, J., Van Daele, M., Heirman, K., Wiemer, G., Molenaar, A., Vandorpe, T., Melnick, D., Hajdas, I., Pino, M., Urrutia, R., and De Batist, M.: The subaqueous landslide cycle in south-central Chilean lakes: The role of tephra, slope gradient and repeated seismic shaking, Sedimentary Geology, 381, 84-105, https://doi.org/10.1016/j.sedgeo.2019.01.002, 2019.
Moernaut, J., Van Daele, M., Strasser, M., Clare, M. A., Heirman, K., Viel, M., Cardenas, J., Kilian, R., Ladrón de Guevara, B., Pino, M., Urrutia, R., and De Batist, M.: Lacustrine turbidites produced by surficial slope sediment remobilization: A mechanism for continuous and sensitive turbidite paleoseismic records, Marine Geology, 384, 159-176, http://dx.doi.org/10.1016/j.margeo.2015.10.009, 2017.

https://doi.org/10.5194/egusphere-2026-2493
Preprint. Discussion started: 1 June 2026

Molenaar, A., Van Daele, M., Huang, J.-J. S., Strasser, M., De Batist, M., Pino, M., Urrutia, R., and Moernaut, J.: Disentangling factors controlling earthquake-triggered soft-sediment deformation in lakes, Sedimentary Geology, 438, https://doi.org/10.1016/j.sedgeo.2022.106200, 2022.

Molenaar, A., Van Daele, M., Vandorpe, T., Degenhart, G., De Batist, M., Urrutia, R., Pino, M., Strasser, M., and Moernaut, J.: What controls the remobilization and deformation of surficial sediment by seismic shaking? Linking lacustrine slope stratigraphy to great earthquakes in South-Central Chile, Sedimentology, 68, 2365-2396, https://www.ncbi.nlm.nih.gov/pubmed/34690376, 2021.

Molenaar, A., Wils, K., Van Daele, M., Daxer, C., Dubois, N., Grießer, A., Oswald, P., Ramisch, A., Strasser, M., and Moernaut, J.: Shaken and Stirred: A Comparative Study of Earthquake-Triggered Soft-Sediment Deformation Structures in Lake Sediments, Geochemistry, Geophysics, Geosystems, 25, https://doi.org/10.1029/2023GC011402, 2024.

Monecke, K., Anselmetti, F. S., Becker, A., Sturm, M., and Giardini, D.: The record of historic earthquakes in lake sediments of Central Switzerland, Tectonophysics, 394, 21-40, https://www.sciencedirect.com/science/article/pii/S0040195104002896, 2004.

Montalva, G. A., Bastías, N., and Leyton, F.: Strong Ground Motion Prediction Model for PGV and Spectral Velocity for the Chilean Subduction Zone, Bulletin of the Seismological Society of America, 112, 348-360, https://doi.org/10.1785/0120210037, 2022.

Montalva, G. A., Bastías, N., and Rodriguez-Marek, A.: Ground-Motion Prediction Equation for the Chilean Subduction Zone, Bulletin of the Seismological Society of America, 107, 901-911, https://doi.org/10.1785/0120160221, 2017.

Moreno, M., Rosenau, M., and Oncken, O.: 2010 Maule earthquake slip correlates with pre-seismic locking of Andean subduction zone, Nature, 467, 198-202, https://doi.org/10.1038/nature09349, 2010.

Moreno, M., Bolte, J., Klotz, J., and Melnick, D.: Impact of megathrust geometry on inversion of coseismic slip from geodetic data: Application to the 1960 Chile earthquake, Geophysical Research Letters, 36, https://doi.org/10.1029/2009GL039276, 2009.

Ndiaye, M., Clerc, N., Gorin, G., Girardclos, S., and Fiore, J.: Lake Neuchâtel (Switzerland) seismic stratigraphic record points to the simultaneous Würmian deglaciation of the Rhône Glacier and Jura Ice Cap, Quaternary Science Reviews, 85, 1-19, https://www.sciencedirect.com/science/article/pii/S0277379113004605, 2014.

Niederstätter, M., Wils, K., Ramisch, A., Haas, J. N., Pomella, H., Szidat, S., Strasser, M., and Moernaut, J.: Strong earthquake in a low seismicity area of the European Southern Alps during Roman Times – A lacustrine paleoseismic evaluation, Quaternary Science Reviews, 357, 109341, https://www.sciencedirect.com/science/article/pii/S0277379125001611, 2025.

Parla, R. and Somala, S. N.: Seismic Ground Motion Amplification in a 3D Sedimentary Basin: Source Mechanism and Intensity Measures, Journal of Earthquake and Tsunami, 16, 2250008, https://doi.org/10.1142/S1793431122500087, 2022.

Pinson, L. J. W., Vardy, M. E., Dix, J. K., Henstock, T. J., Bull, J. M., and Maclachlan, S. E.: Deglacial history of glacial lake windermere, UK: implications for the central British and Irish Ice Sheet, Journal of Quaternary Science, 28, 83-94, https://doi.org/10.1002/jqs.2595, 2013.

Pitilakis, K., Riga, E., and Anastasiadis, A.: New code site classification, amplification factors and normalized response spectra based on a worldwide ground-motion database, Bulletin of Earthquake Engineering, 11, 925-966, https://doi.org/10.1007/s10518-013-9429-4, 2013.

Praet, N., Moernaut, J., Van Daele, M., Boes, E., Haeussler, P. J., Strupler, M., Schmidt, S., Loso, M. G., and De Batist, M.: Paleoseismic potential of sublacustrine landslide records in a high-seismicity setting (south-central Alaska), Marine Geology, 384, 103-119, https://www.sciencedirect.com/science/article/pii/S0025322716300767, 2017.

Raptakis, D. G., Manakou, M. V., Chávez-García, F. J., Makra, K. A., and Pitilakis, K. D.: 3D configuration of Mygdonian basin and preliminary estimate of its site response, Soil Dynamics and Earthquake Engineering, 25, 871-887, https://www.sciencedirect.com/science/article/pii/S0267726105001156, 2005.

Richards, P. G. and Menke, W.: The apparent attenuation of a scattering medium, Bulletin of the Seismological Society of America, 73, 1005-1021, https://doi.org/10.1785/BSSA0730041005, 1983.

Rodríguez-Pascua, M. A., Calvo, J. P., De Vicente, G., and Gómez-Gras, D.: Soft-sediment deformation structures interpreted as seismites in lacustrine sediments of the Prebetic Zone, SE Spain, and their potential use as indicators of earthquake magnitudes during the Late Miocene, Sedimentary Geology, 135, 117-135, https://www.sciencedirect.com/science/article/pii/S0037073800000671, 2000.

https://doi.org/10.5194/egusphere-2026-2493
Preprint. Discussion started: 1 June 2026

Roten, D., Fäh, D., Cornou, C., and Giardini, D.: Two-dimensional resonances in Alpine valleys identified from ambient vibration wavefields, Geophysical Journal International, 165, 889-905, https://doi.org/10.1111/j.1365-246X.2006.02935.x, 2006.

Sawyer, D. E. and DeVore, J. R.: Elevated shear strength of sediments on active margins: Evidence for seismic strengthening, Geophysical Research Letters, 42, 10,216-210,221, https://doi.org/10.1002/2015GL066603, 2015.

Seibert, C., McHugh, C., Paola, C., Seeber, L., and Tucker, J.: Surficial sediment remobilization by shear between sediment and water above tsunamigenic megathrust ruptures: experimental study, Earth Surf. Dynam., 13, 341-348, https://esurf.copernicus.org/articles/13/341/2025/, 2025.

Semblat, J. F., Duval, A. M., and Dangla, P.: Seismic site effects in a deep alluvial basin: numerical analysis by the boundary element method, Computers and Geotechnics, 29, 573-585, https://www.sciencedirect.com/science/article/pii/S0266352X02000174, 2002.

Semblat, J. F., Kham, M., Parara, E., Bard, P. Y., Pitilakis, K., Makra, K., and Raptakis, D.: Seismic wave amplification: Basin geometry vs soil layering, Soil Dynamics and Earthquake Engineering, 25, 529-538, https://www.sciencedirect.com/science/article/pii/S0267726105000436, 2005.

Shen, H., Liu, Y., Li, X., Li, H., Wang, L., and Huang, W.: The combined amplification effects of topography and stratigraphy of layered rock slopes under vertically and obliquely incident seismic waves, Soil Dynamics and Earthquake Engineering, 193, https://doi.org/10.1016/j.soildyn.2025.109331, 2025.

Shynkarenko, A., Lontsi, A. M., Kremer, K., Bergamo, P., Hobiger, M., Hallo, M., and Fäh, D.: Investigating the subsurface in a shallow water environment using array and single-station ambient vibration techniques, Geophysical Journal International, 227, 1857-1878, https://doi.org/10.1093/gji/ggab314, 2021.

Stewart, J. P., Klimis, N., Savvaidis, A., Theodoulidis, N., Zargli, E., Athanasopoulos, G., Pelekis, P., Mylonakis, G., and Margaris, B.: Compilation of a Local VS Profile Database and Its Application for Inference of VS30 from Geologic- and Terrain-Based Proxies, Bulletin of the Seismological Society of America, 104, 2827-2841, https://doi.org/10.1785/0120130331, 2014.

Strasser, M., Anselmetti, F. S., Fäh, D., Giardini, D., and Schnellmann, M.: Magnitudes and source areas of large prehistoric northern Alpine earthquakes revealed by slope failures in lakes, Geology, 34, 1005-1008, https://doi.org/10.1130/G22784A.1, 2006.

Strasser, M., Stegmann, S., Bussmann, F., Anselmetti, F. S., Rick, B., and Kopf, A.: Quantifying subaqueous slope stability during seismic shaking: Lake Lucerne as model for ocean margins, Marine Geology, 240, 77-97, https://doi.org/10.1016/j.margeo.2007.02.016, 2007.

Taborda, R. and Roten, D.: Physics-Based Ground-Motion Simulation, in: Encyclopedia of Earthquake Engineering, 1-33, 2015.

Tarbali, K. and Bradley, B. A.: The effect of causal parameter bounds in PSHA-based ground motion selection, Earthquake Engineering & Structural Dynamics, 45, 1515-1535, https://doi.org/10.1002/eqe.2721, 2016.

Van Daele, M., Bertrand, S., Meyer, I., Moernaut, J., Vandoorne, W., Siani, G., Tanghe, N., Ghazoui, Z., Pino, M., Urrutia, R., and De Batist, M.: Late Quaternary evolution of Lago Castor (Chile, 45.6°S): Timing of the deglaciation in northern Patagonia and evolution of the southern westerlies during the last 17 kyr, Quaternary Science Reviews, 133, 130-146, https://doi.org/10.1016/j.quascirev.2015.12.021, 2016.

Van Daele, M., Moernaut, J., Doom, L., Boes, E., Fontijn, K., Heirman, K., Vandoorne, W., Hebbeln, D., Pino, M., Urrutia, R., Brümmer, R., and De Batist, M.: A comparison of the sedimentary records of the 1960 and 2010 great Chilean earthquakes in 17 lakes: Implications for quantitative lacustrine palaeoseismology, Sedimentology, 62, 1466-1496, https://doi.org/10.1111/sed.12193, 2015.

Vandekerkhove, E., Van Daele, M., Praet, N., Cnudde, V., Haeussler, P. J., and De Batist, M.: Flood-triggered versus earthquake-triggered turbidites: A sedimentological study in clastic lake sediments (Eklutna Lake, Alaska), Sedimentology, 67, 364-389, https://doi.org/10.1111/sed.12646, 2020.

Vanneste, K., Wils, K., and Van Daele, M.: Probabilistic Evaluation of Fault Sources Based on Paleoseismic Evidence From Mass-Transport Deposits: The Example of Aysén Fjord, Chile, Journal of Geophysical Research: Solid Earth, 123, 9842-9865, https://doi.org/10.1029/2018JB016289, 2018.

Wald, D. J. and Allen, T. I.: Topographic Slope as a Proxy for Seismic Site Conditions and Amplification, Bulletin of the Seismological Society of America, 97, 1379-1395, https://doi.org/10.1785/0120060267, 2007.

https://doi.org/10.5194/egusphere-2026-2493
Preprint. Discussion started: 1 June 2026

Wetzler, N., Marco, S., and Heifetz, E.: Quantitative analysis of seismogenic shear-induced turbulence in lake sediments, Geology, 38, 303-306, https://doi.org/10.1130/G30685.1, 2010.

Wiemer, G. and Kopf, A.: Influence of diatom microfossils on sediment shear strength and slope stability, Geochemistry, Geophysics, Geosystems, 18, 333-345, https://doi.org/10.1002/2016GC006568, 2017.

Wiemer, G., Dziadek, R., and Kopf, A.: The enigmatic consolidation of diatomaceous sediment, Marine Geology, 385, 173-184, https://www.sciencedirect.com/science/article/pii/S0025322717300142, 2017.

Wiemer, G., Moernaut, J., Stark, N., Kempf, P., De Batist, M., Pino, M., Urrutia, R., de Guevara, B. L., Strasser, M., and Kopf, A.: The role of sediment composition and behavior under dynamic loading conditions on slope failure initiation: a study of a subaqueous landslide in earthquake-prone South-Central Chile, International Journal of Earth Sciences, 104, 1439-1457, https://doi.org/10.1007/s00531-015-1144-8, 2015.

Wilhelm, B., Nomade, J., Crouzet, C., Litty, C., Sabatier, P., Belle, S., Rolland, Y., Revel, M., Courboulex, F., Arnaud, F., and Anselmetti, F. S.: Quantified sensitivity of small lake sediments to record historic earthquakes: Implications for paleoseismology, Journal of Geophysical Research: Earth Surface, 121, 2-16, https://doi.org/10.1002/2015jf003644, 2016.

Wils, K., Montalva, G., Van Daele, M., De Batist, M., and Moernaut, J.: Peak Ground Velocity and Shaking Duration Control Coseismic Surficial Sediment Remobilization on Lacustrine Slopes and Emplacement of Seismoturbidites, Seismological Research Letters, https://doi.org/10.1785/0220240487, 2026.

Yang, Z., Elgamal, A., and Parra, E.: Computational Model for Cyclic Mobility and Associated Shear Deformation, Journal of Geotechnical and Geoenvironmental Engineering, 129, 1119-1127, https://doi.org/10.1061/(ASCE)1090-0241(2003)129:12(1119), 2003.

Yang, H. Modeling Seismic Site Response in Lake Riñihue [Data set]. Zenodo. https://doi.org/10.5281/zenodo.19660999, 2026